LGL-1 and the RhoGAP protein PAC-1 redundantly control polarization of the *C. elegans* embryonic epidermal epithelium

Olga D. Jarosińska[1], Amalia Riga[1], Hala Zahreddine Fahs[2,3], Joren M. Woeltjes[1], Ruben Schmidt[1], Fathima S. Refai[2,4], Suma Gopinadhan[2], Kristin C. Gunsalus[2,3] and Mike Boxem[1]

- [1]Institute of Biodynamics and Biocomplexity, Department of Biology, Utrecht University, Padualaan 8, 3584 CH Utrecht, The Netherlands
- [2]Center for Genomics and Systems Biology, New York University Abu Dhabi, United Arabic Emirates
- [3]Department of Biology and Center for Genomics and Systems Biology, New York University, New York, USA
- [4]Dipartimento di Medicina, Università di Udine, 33100 Udine, Italy

Keywords: epithelia; embryogenesis; cell polarity; Lgl; RhoGAP19D; PAC-1

Correspondence: Mike Boxem, m.boxem@uu.nl

Abstract

The formation of an apical–basal axis of polarity is essential for the organization and functioning of epithelial cells. Apical–basal polarity is established by cortical polarity proteins that define the apical, junctional, and basolateral domains. While cortical polarity proteins are highly conserved and present in most epithelia, the mechanisms that establish polarity and the requirements for canonical polarity factors can vary between tissues and organisms. For example, the basolateral polarity protein lethal giant larvae (Lgl) is essential for the polarization of most *Drosophila* epithelia, yet is dispensable for epithelial polarization and viability in *C. elegans*.

To better understand the epithelial polarity program in *C. elegans*, we performed a whole-genome RNAi screen for synthetic lethality with an *lgl-1* deletion mutant. We found that combined loss of LGL-1 and the RhoGAP protein PAC-1 (RhoGAP19D in flies) leads to embryonic lethality due to defects in elongation and rupturing of the epidermis. We observed mislocalization of junctional proteins to the lateral domain of epidermal cells, presumably weakening tissue integrity. Furthermore, we observed expansion of the apical domain, sporadic aPKC mislocalization, and localization of the basolateral polarity protein LET-413^{Scribble} in patches surrounded by DLG-1$^{\text{Discs large}}$. These observations indicate that the combined loss of LGL-1 and PAC-1 leads to an overactivity of apical domain specifying factors. Consistent with this, partial inactivation of the apical polarity regulators aPKC or CDC-42 reduced the lethality of *pac-1(RNAi); lgl-1(null)* animals. Taken together, our findings identify *pac-1* and *lgl-1* as redundant inhibitors of apical polarity factors. While their relative contribution to the epithelial polarity program differ from fly epithelia, the canonical apical-basal polarity machinery is thus active in the embryonic epidermis of *C. elegans* – providing new insight into how conserved mechanisms are adapted across species.

Introduction

The form and functioning of epithelial cells are dependent on their organization along an apical–basal axis of polarity. Epithelial polarity is established by conserved polarity regulators that engage in mutually antagonistic interactions to establish distinct apical, lateral, and basal membrane domains, and position cell junctions [1–4]. Specification of the apical domain involves the activities of the partitioning defective proteins Par3 (Bazooka in *Drosophila*) and Par6, atypical protein kinase C (aPKC), the small Rho GTPase Cdc42, the transmembrane protein Crumbs, and its intracellular adapter Pals1 (Stardust in *Drosophila*). Formation of the basolateral domain depends on the Scribble module proteins Scribble (Scrib), Discs large (Dlg), and Lethal giant larvae (Lgl), as well as on the kinase Par1.

Mutual inhibition between aPKC and Lgl plays a central role in the network of antagonistic interactions that establish apical–basal polarity. At the apical domain, aPKC phosphorylates a range of polarity proteins to mediate their exclusion from the plasma membrane, including Lgl [5–9]. aPKC strongly interacts with Par6, and formation of an Par6/aPKC complex is necessary for both localization and activity of aPKC [10–12]. Par6 can locate aPKC to the apical membrane domain by interacting with Par3 or Cdc42, both of which can bind Par6 and recruit Par6/aPKC to the membrane [11,13–18]. Full activation of the kinase activity of aPKC is promoted by binding to Cdc42, and in the *C. elegans* zygote Par6/aPKC have been shown to shuttle between an inactive PAR-3 complex and an active CDC-42 complex [11,12,14,19–22]. Binding of Par6/aPKC to Cdc42 also increases the affinity of Par6 for Crumbs, and handoff from Cdc42 to Crumbs may further stabilize active Par6/aPKC at the membrane [15,20,23]. At the basolateral domain, Lgl is required to antagonize the activity of Par6/aPKC [24–26]. Lgl forms a ternary complex with Par6/aPKC via multiple interaction interfaces [8,27,28]. However, it is still unclear if the antagonistic activity towards aPKC is based on inhibition of kinase activity or if Lgl prevents phosphorylation of other aPKC targets by competitively keeping aPKC engaged with processive Lgl phosphorylation.

While these cortical polarity determinants are highly conserved in metazoans, much of our understanding of their functioning in apical–basal polarity establishment in epithelia is based on studies in *Drosophila.* It is clear, however, that there is considerable variation in the mechanisms that establish apical–basal polarity between different organisms and between different epithelial tissues in the same organism. For example, in *Drosophila*, not all epithelial tissues that express Crumbs depend on it to establish polarity [29–31], while all three *C. elegans* Crumbs family members collectively are dispensable for polarity establishment [32,33]. Recent studies in

Drosophila have also shown that the enterocytes of the midgut do not require any of the canonical polarity factors and appear to use a different mode of polarization [34]. It is important therefore to investigate the mechanisms that underly apical–basal polarization in different developmental and organismal contexts, and determine how universal the roles of different polarity modules are.

The *C. elegans* Lgl ortholog LGL-1 is a striking example of how polarity proteins may vary in their importance in epithelial polarization. While *Drosophila* Lgl is essential for epithelial polarity establishment, *C. elegans* lacking LGL-1 are viable and show no defects in polarity establishment. [35,36]. In the one cell embryo, the lack of an essential role for LGL-1 may be explained by the presence of the *C. elegans* specific protein PAR-2, which acts redundantly with LGL-1 [35,36]. However, expression of PAR-2 is limited to the germ lineage while LGL-1 is broadly expressed [35–37]. LGL-1 may also antagonize aPKC in the spermatheca, as *lgl-1* mutants were found as suppressors of a temperature sensitive *aPKC* allele that causes junction breaks in the spermatheca and leads to sterility [38]. It is not known, however, whether LGL-1 functions similarly in other epithelia or why loss of LGL-1 does not cause epithelial polarity defects.

Another polarity regulator whose functioning may differ between *Drosophila* and *C. elegans* is the RhoGAP protein PAC-1 (RhoGAP19D in *Drosophila* and ARHGAP21 in mammals). PAC-1 was identified as a regulator of radial polarization of *C. elegans* blastomeres, mediating the asymmetric enrichment of Par6/aPKC to the outer contact-free cell surfaces [39]. E-cadherin-dependent recruitment of PAC-1 to sites of cell–cell contact is thought to locally inactivate CDC-42, restricting recruitment of Par6/aPKC by CDC-42 to the outer surfaces [39,40]. Additionally, in epidermal cells of the embryo, PAC-1 is involved in regulating junctional actin organization and the levels of AJ proteins, likely also by regulating CDC-42 activity [41]. However, *pac-1* is not an essential gene. Loss of *pac-1* causes defects in cell positioning during gastrulation but >90% of embryos hatch and develop normally [41]. In contrast, *Drosophila* RhoGAP19D was identified as an essential protein that antagonizes aPKC at the lateral domain [42]. RhoGAP19D is recruited to the lateral domain of follicle cells by the E-cadherin complex, and its loss leads to ectopic lateral Cdc42 activity, increased Par6/aPKC activity, and expansion of the apical domain. *rhogap19d* mutants die at various stages of development, indicating a broad role of RhoGAP19D in epithelial polarization [42].

Here, we investigate the role of LGL-1 in polarity establishment in *C. elegans*. We performed an RNAi-based synthetic lethality screen in an *lgl-1* deletion background and found that the

105 combined loss of *lgl-1* and *pac-1* leads to a fully penetrant lethal phenotype, with most animals
106 arresting at the embryonic elongation stage with frequent rupturing of the epidermis. The
107 rupturing is likely due to severe defects apical–basal polarization and apical junction formation in
108 the epidermis. We show that the lethality of combined *lgl-1* and *pac-1* loss can be reduced by
109 lowering the levels or activity of the apical polarity proteins CDC-42 or aPKC. These experiments
110 are the first demonstration that LGL-1 and PAC-1 act together in epithelial polarization in *C.*
111 *elegans*, likely by redundantly controlling aPKC activity. As LGL-1 has now been shown to act
112 redundantly with a second polarity regulator in two tissues, we speculate that such redundancy
113 is a general feature of LGL-1 in *C. elegans*. Our data thus imply that differences in essentiality of
114 cortical polarity regulators reflect changes in the strengths of the wiring of the different
115 connections in the epithelial polarity network, rather than major differences in the mode of
116 polarization.

117 Results

118 The RhoGAP protein PAC-1 acts redundantly with LGL-1 in embryonic 119 development

120 Previously, LGL-1 was shown to act redundantly with PAR-2 during polarity establishment in the
121 one cell embryo. To identify genes that may act redundantly with *lgl-1* in other developmental
122 stages, we performed an RNAi-based enhancer screen. We first generated the *lgl-1(mib44)*
123 deletion allele by replacing most of the *lgl-1* coding sequence with *GFP* expressed from the *myo-2*
124 promoter (Fig. S1A). We then used this strain to perform a whole-genome feeding RNAi screen
125 using the Ahringer feeding library in an automated robotics pipeline [43,44] (Fig. S1B). We
126 identified 79 RNAi clones that caused stronger fitness or developmental defects in *lgl-1(mib44)*
127 animals compared to wild-type controls. We discarded 27 of these that are frequently identified
128 as enhancers in the screening pipeline as likely false positives. Of the remaining clones, 5
129 retested positive by feeding RNAi on plates using sequence-verified RNAi clones (Fig. S1C). We
130 decided to focus on the RhoGAP encoding gene *pac-1* because of the strong synthetic lethality
131 displayed with *lgl-1* and its previously described roles in radial polarization of early embryonic
132 blastomeres and regulation of CDC-42 [28,39,45,45].

133 To further investigate the interaction between *pac-1* and *lgl-1*, we generated the *pac-1(mib269)*
134 deletion allele, which removes the entire *pac-1* coding sequence. We also generated a second *lgl-*
135 *1* deletion allele *(mib201)*, replacing the GFP in *mib44* with BFP to mitigate imaging problems due

136 to the extreme brightness of *Pmyo-2::GFP* (Fig. S1A). The *lgl-1* and *pac-1* deletion strains are viable
137 and behave as previously described strains carrying loss-of-function alleles. Deletion of *lgl-1* does
138 not cause apparent developmental defects [35,36], while loss of *pac-1* causes ~10% embryonic
139 lethality with the remain animals developing normally [39,41] (Fig. 1A). In contrast, injection of
140 *pac-1* dsRNA in *lgl-1(mib201)* or of *lgl-1* dsRNA in *pac-1(mib269)* resulted in nearly complete
141 embryonic lethality (Fig. 1A). To further confirm the genetic interaction, we generated animals
142 homozygous for *pac-1(mib269)* and heterozygous for *lgl-1(mib44)* and examined their offspring.
143 Interestingly, progeny from these *pac-1(mib269); lgl-1(mib44)/+* parents showed 43% embryonic
144 or early larval lethality rather than the expected 25%, indicating that the *lgl-1* deletion allele is
145 partially haplo-insufficient (Fig. 1A). Consistent with this interpretation, among the surviving
146 animals, 45% expressed GFP, and hence carried at least one copy of the *lgl-1* deletion allele,
147 rather than the expected 67%.

148 Differential interference contrast (DIC) microscopy of *lgl-1(mib201); pac-1(RNAi)* and *pac-*
149 *1(mib269); lgl-1(mib44)* embryos revealed that most arrest during the elongation phase of
150 embryonic development (Fig. 1B), with a bulging epidermis and frequent ruptures of the
151 epidermis (Fig. 1C). Together, these experiments show that *pac-1* and *lgl-1* are redundantly
152 required for embryonic development. As inactivation of *pac-1* by RNAi or gene deletion caused
153 indistinguishable results, most further experiments were done with *pac-1(RNAi)* for ease of use.

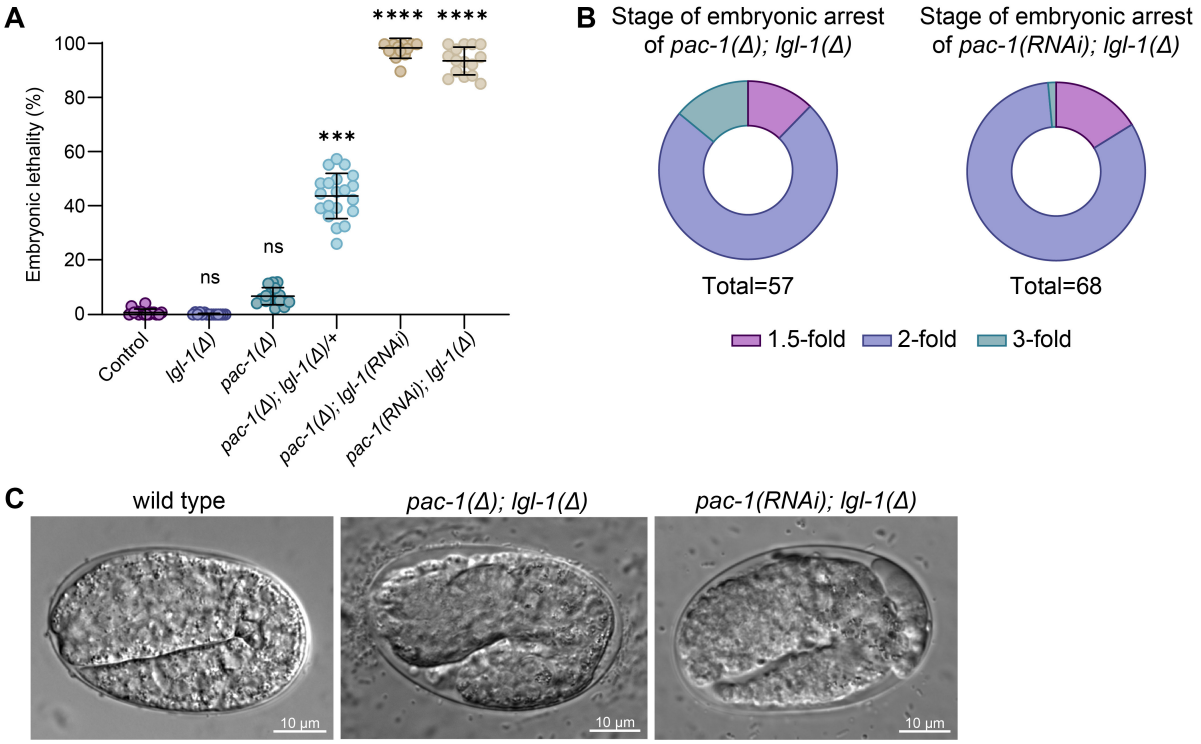

154

155 **Figure 1. The RhoGAP protein PAC-1 acts redundantly with LGL-1 in embryonic development.**
156 (**A**) Embryonic lethality observed in progeny of animals of indicated genotypes. Data is represented
157 as mean ± SD and analyzed with a Kruskal-Wallis test followed by Dunn's multiple pairwise
158 comparison test; ns = $p > 0.05$, *** = $p < 0.0005$, **** = $p < 0.0001$. (**B**) Stage of embryonic arrest of
159 double mutant *lgl-1(mib201); pac-1(RNAi)* and *pac-1(mib269); lgl-1(mib44)* embryos. Because of the
160 haplo-insufficiency of *lgl-1* loss, homozygous *pac-1(mib269); lgl-1(mib201)* embryos were derived from
161 *pac-1(mib269); lgl-1::GFP(crk66)/lgl-1(mib201)* parents, so they could be unambiguously identified by
162 the absence of GFP expression. (**C**) Representative DIC images of wild-type, *pac-1(mib269); lgl-*
163 *1(mib44)*, and *pac-1(RNAi); lgl-1(mib201)* embryos. Strains used: CGC1, BOX1221, BOX919.

164 PAC-1 and LGL-1 redundantly control the positioning of apical junctions

165 Embryonic elongation is dependent on adherens junctions, and the defects we observe in
166 embryos lacking *lgl-1* and *pac-1,* including the 2-fold arrest and rupturing of the epidermis, are
167 also observed in embryos with defects in junctional integrity [46–48]. Moreover, loss of PAC-1
168 was previously shown to block elongation in embryos carrying the hypomorphic HMP-1/α-
169 catenin mutant *fe4,* which has reduced actin binding capability [41,49]. We therefore investigated
170 if combined loss of *pac-1* and *lgl-1* results in defects in junctional integrity in embryonic
171 epidermal cells. We visualized the distribution of each of the three junctional complexes [50] in
172 *pac-1(RNAi); lgl-1(mib201)* embryos using a representative protein endogenously fused to a
173 fluorescent protein. We imaged HMR-1::GFP (E-cadherin) from the cadherin/catenin complex
174 (CCC), AFD-1::GFP (Afadin) from the SAX-7/MAGI-1/AFD-1 complex (SMAC) and DLG-1::mCherry
175 from the DLG-1/AJM-1 complex (DAC) [50].

176 Consistent with our DIC observations, time-lapse imaging of DLG-1::mCherry or a membrane
177 marker, the PH domain fused to GFP (PH::GFP), in *lgl-1(mib201); pac-1(RNAi)* embryos showed that
178 most double mutant embryos completed ventral closure and arrested during elongation with
179 rupturing of the epidermis visible as expulsion of internal cells (Fig. S2A and Videos S1, 2). We
180 observed ruptures on both the ventral and dorsal side of the embryos, and at multiple positions
181 along the anterior–posterior body axis. Thus, the weakening of the epidermis does not appear to
182 be limited to any particular region.

183 In 3D confocal imaging, we observed aberrant lateral spreading of each of the three junctional
184 proteins, in addition to their normal subapical localization (visible as double lines in maximum
185 intensity projections, see arrowheads in Fig. 2A). The defects were most severe for DLG-1, which
186 also showed gaps in the normally continuous junctional band (arrows in Figs. 2A and S2B). To

187 better visualize the basolateral mislocalization, we imaged DLG-1 together with PH::GFP. In cross-
188 sections of *pac-1(RNAi); lgl-1(mib201)* embryos, DLG-1 was spread along the lateral membrane
189 compared to the tight subapical localization observed in controls expressing wild-type *lgl-1* and
190 *pac-1* (Fig 2B). Finally, we rendered image stacks of embryos expressing HMR-1::GFP and DLG-
191 1::mCherry in 3D. Control animals showed the expected subapical localization of both proteins,
192 with HMR-1 signal appearing slightly more apical than DLG-1 (Fig. 2C, junctions 'i' and 'ii').
193 However, in *pac-1(RNAi); lgl-1(mib201)* embryos, DLG-1 and HMR-1 were spread along the lateral
194 membrane (Fig. 2C, junction 'iii'). The two proteins did not mix completely but showed remaining
195 organization with regions expressing predominantly DLG-1 being flanked by HMR-1 signal.
196 Additionally, we observed ring-like structures where junctional material appeared to encircle a
197 junction-free area on the lateral domain (Fig. 2C, junction 'iv').

198 To determine if the defects in junction formation are due to a loss of stability of DLG-1 protein at
199 the membrane, we performed fluorescence recovery after photobleaching (FRAP) experiments
200 using a DLG-1::mCherry endogenous fusion protein. The recovery of DLG-1 was not affected by
201 loss of *lgl-1* and *pac-1,* indicating that the junctional defects are not due to reduced stability of
202 DLG-1 at the membrane (Fig. S2C, D). Furthermore, time-lapse imaging of DLG-1 showed that
203 regions lacking DLG-1 protein remained stable over time (Videos S3, 4). Thus, the DLG-1
204 positioning defects observed in *pac-1; lgl-1* embryos do not appear to stem from a general
205 change in stability of DLG-1 at the membrane, but rather from defects in specifying the
206 positioning of junctional components.

207 Finally, loss of *pac-1* was previously shown to increase embryonic lethality in the genetically
208 sensitized *hmp-1(fe4)* background. The *fe4* allele encodes a HMP-1$^{\alpha\text{-catenin}}$ variant with reduced
209 actin binding that has been used to identify multiple genes that play a role in adherens junction
210 (AJ) functioning [49,51–53]. To determine if *lgl-1* may directly affect AJs, we inactivated *lgl-1* in the
211 *hmp-1(fe4)* background. In contrast to *pac-1*, we did not observe any changes in survival of *hmp-*
212 *1(fe4)* progeny after injection of *lgl-1* dsRNA (Fig. 2D). This observation argues against a primary
213 role for *lgl-1* in regulating cell junctions.

214 In summary, the combined loss of *lgl-1* and *pac-1* leads to severe defects in the integrity of apical
215 cell junctions, which are likely the cause of the epidermal rupturing and elongation arrest. Unlike
216 *pac-1*, *lgl-1* does not synergize with junction compromised *hmp-1(fe4)* mutants, indicating that *lgl-*
217 *1* does not directly regulate AJ formation or functioning.

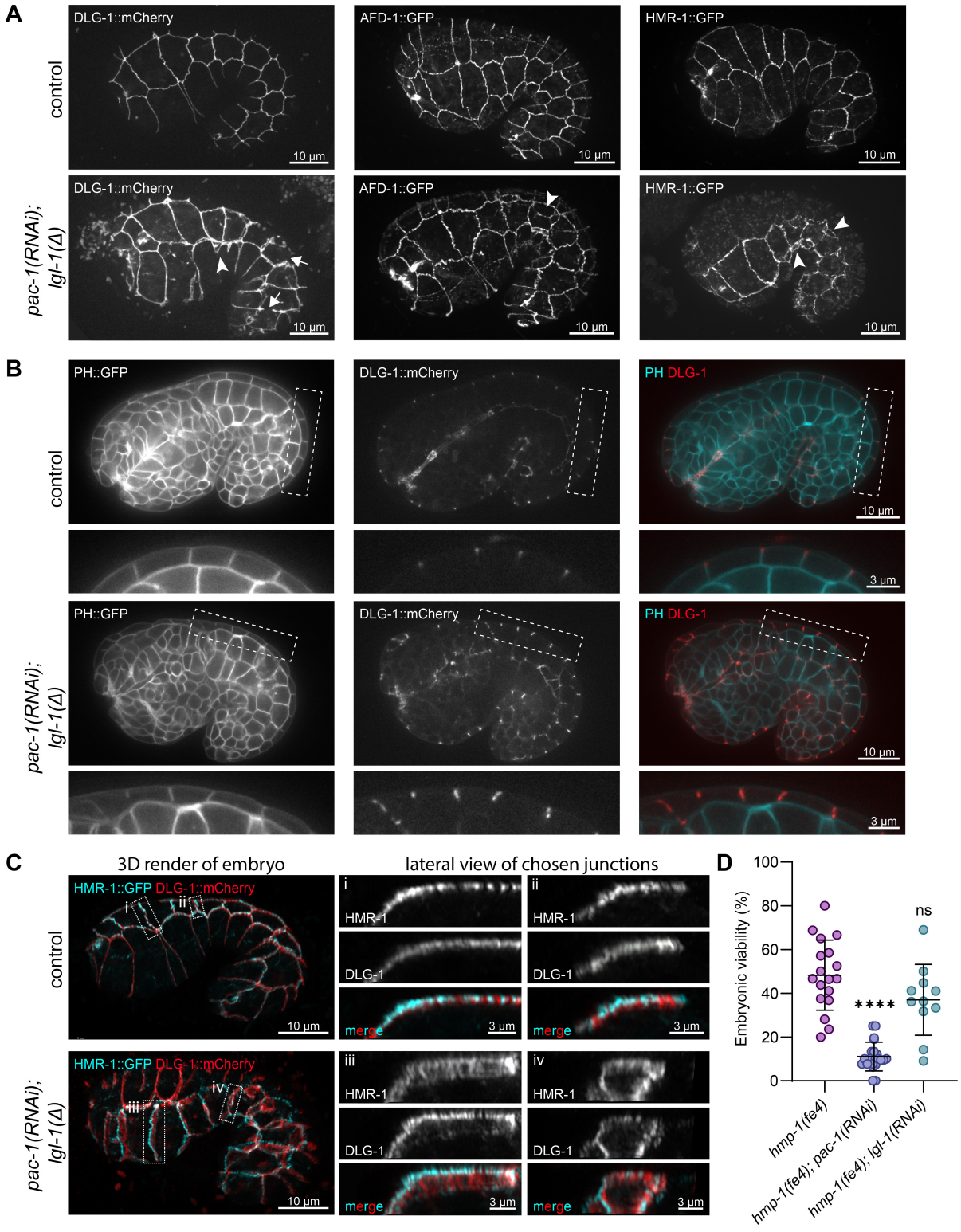

Figure 2. Aberrant localization of junctional marker proteins in *lgl-1(mib201); pac-1(RNAi)* embryos compared to controls. (**A**) Maximum intensity projections of 3D stacks taken with a spinning disc confocal microscope showing the localization of DLG-1::mCherry, AFD-1::GFP and HMR-1::GFP. Arrowheads indicate sites of additional basal junctional signal. Asterisk indicates gap in junctional band. Strains used: BOX804, BOX940, BOX258, BOX943. (**B**) Single plane internal view

224 showing the localization of DLG-1::mCherry in respect to the PH::GFP membrane marker. Enlarged
225 versions of the boxed regions are shown below each panel. Images were taken on a spinning disc
226 confocal microscope. Strains used: BOX1076, BOX1077. (**C**) 3D rendering of Airyscan confocal images
227 showing DLG-1::mCherry and HMR-1::GFP. Lateral views of the boxed junctions are depicted to the
228 right of the whole embryo images. Strains used: BOX804, BOX940. (**D**) Percentage of lethal embryos
229 from *hmp-1(fe4)* and upon knockdown of *lgl-1* or *pac-1*. Data is represented as mean ± SD and
230 analyzed with a Brown-Forsythe and Welch ANOVA test followed by Dunnett's T3 multiple
231 comparison test; ns = $p > 0.05$, **** = $p < 0.0001$.

232 Loss of LGL-1 and PAC-1 disrupts apical–basal polarity in the embryonic 233 epidermis

234 Since both LGL-1 and PAC-1 are thought to directly or indirectly regulate aPKC localization or
235 activity, the junctional defects in *pac-1; lgl-1* embryos may be a result of defects in apical–basal
236 polarization. To investigate this, we examined the localization pattern of aPKC using an
237 endogenous N-terminal GFP::aPKC fusion protein (Castiglioni et al., 2020a). Consistent with
238 previous reports, GFP::aPKC was enriched at the apical cortex and at cell junctions of epidermal
239 epithelial cells during elongation (Fig. 3A). In *pac-1(RNAi); lgl-1(mib201)* embryos, aPKC occupied a
240 broader region apical to cell junctions, indicating enlargement of the apical domain (arrows in
241 Fig. 3A and Fig. S3A). Consistent with an expansion of the apical domain, cells appeared more
242 dome shaped than in wild-type controls (Fig. 3B). To quantify this, we determined the tortuosity
243 of the apical domains, defined as the ratio of the length of the apical surface to the direct
244 distance between its end points (the junctions). We indeed observed a significantly increased
245 tortuosity of 1.06 compared to 1.03 in controls (Fig. 3C).

246 In addition to the expanded apical domain, we found that in areas with ectopic lateral DLG-1
247 distribution, aPKC also localized laterally, directly adjacent to or interspersed with the DLG-1
248 signal. This was especially apparent in lateral regions where DLG-1 was present in a ring-like
249 structure (arrowheads in Fig. 3A and Fig. S3A). To further investigate the polarization in these
250 regions, we examined the localization of LET-413^{Scribble}, which is normally uniformly distributed
251 along the basolateral membrane and enriched at junctions. In *pac-1(RNAi); lgl-1(mib201)* embryos,
252 we observed lateral regions in which LET-413 was absent (Fig. 3D). Strikingly, in lateral areas with
253 a ring-like distribution of DLG-1, LET-413 was enriched within the ring and absent outside of it
254 (Fig. 3D and S3B). Thus, loss of *pac-1* and *lgl-1* can lead to patches of basolateral identity
255 surrounded by junctional material and aPKC.

256 As aPKC can be recruited by CDC-42, and PAC-1 is a RhoGAP for CDC-42, we also attempted to
257 determine if loss of LGL-1 and PAC-1 affects the activity of CDC-42 using a biosensor consisting of
258 the WSP-1 G-protein binding domain fused to GFP expressed from the *cdc-42* promoter
259 (GFP::GBD$_{WSP-1}$) [41,55,56]. However, the GFP::GBD$_{WSP-1}$ biosensor was strongly expressed and
260 uniformly localized to the entire cell cortex of embryonic epidermal cells, and therefore not likely
261 to be able to detect the local changes in CDC-42 activity expected from a loss of PAC-1. Indeed,
262 we observed no significant changes in apical GFP::GBD$_{WSP-1}$ membrane levels upon inactivation of
263 *lgl-1* and *pac-1* (Fig. S3C, D).

264 Taken together, these data indicate that the combined loss of LGL-1 and PAC-1 results in a shift
265 in the balance of apical vs. basolateral specifying activities towards promotion of apical identity.
266 In most cells, this manifests as an expansion of the apical domain but in severe cases this can
267 lead to a largely apicalized cell membrane with small patches of basolateral domain (Fig. 3E).

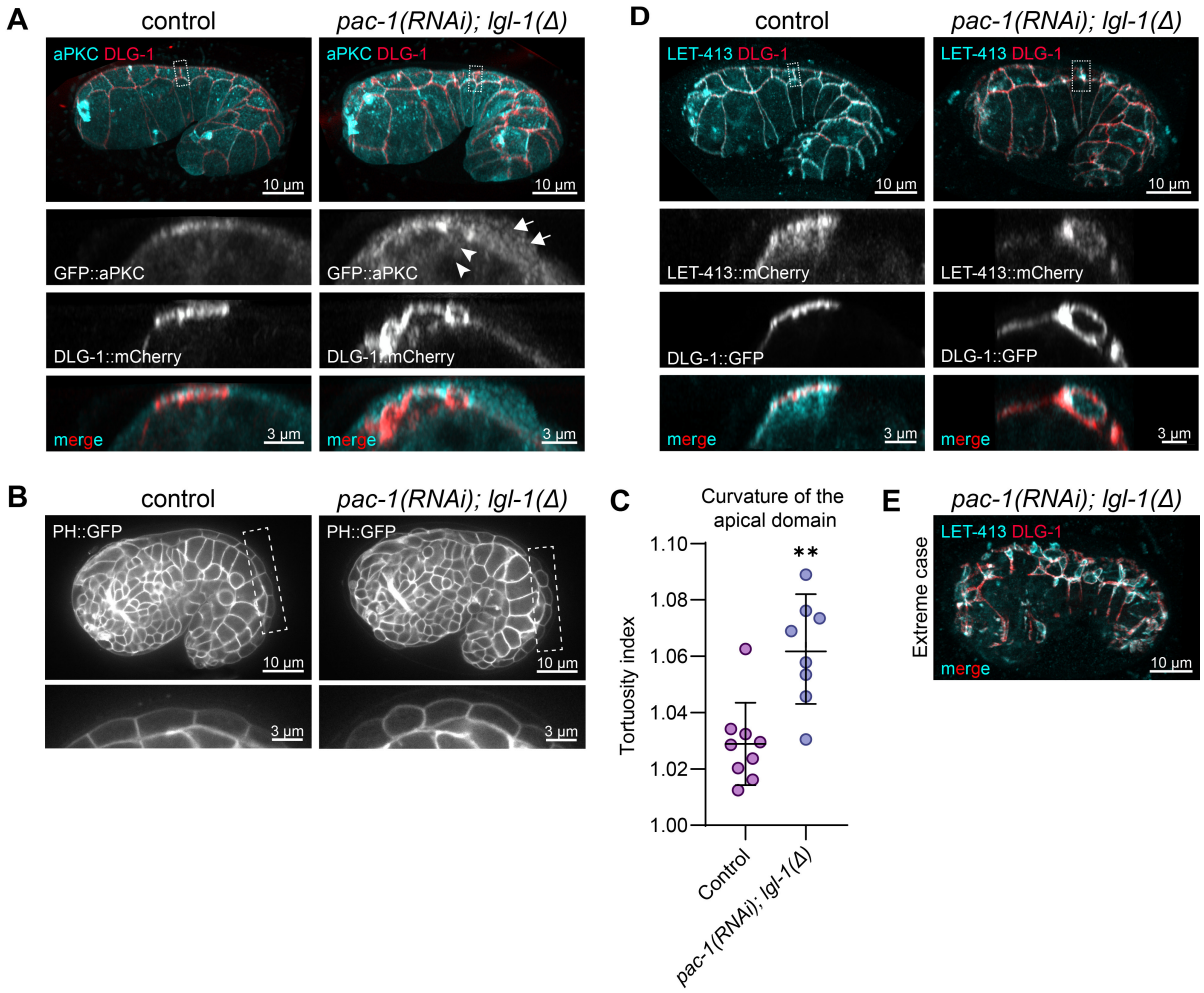

268

269 **Figure 3. Loss of *lgl-1* and *pac-1* disrupts apical-basal polarity in the embryonic epidermis.** (**A**)
270 3D rendering of Airyscan confocal images showing DLG-1::mCherry and aPKC::GFP. Lateral views of

271 the boxed regions are depicted below the whole embryo images. Asterisk indicates expanded aPKC
272 domain and arrowheads indicate lateral mislocalization of aPKC. Strains used: BOX1160, BOX1161.
273 (**B**) Single plane internal view showing the curvature of the apical domain of the epidermal cells using
274 the PH::GFP as membrane marker. Enlarged versions of the boxed regions are shown below each
275 panel. Images were taken on a spinning disc confocal microscope. Strains used: BOX1076, BOX1077.
276 (**C**) Quantification of the tortuosity of the epidermal cell apical domain. Each point is the average
277 tortuosity of ≥10 cells in the embryo. Data is represented as mean ± SD and analyzed using the
278 unpaired t test; ** = $p \leq 0.010$. (**D**) 3D rendering of Airyscan confocal images showing DLG-1::GFP and
279 LET-413::mCherry. Lateral views of the boxed junctions are depicted below the whole embryo
280 images. Strains used: BOX527, BOX1100. (**E**) 3D rendering of Airyscan confocal image showing an
281 extreme case of DLG-1::GFP and LET-413::mCherry mislocalization. Strain used: BOX1100.

282 PAC-1 and LGL-1 act in parallel to antagonize aPKC and CDC-42

283 If the loss of *lgl-1* and *pac-1* leads to higher level of apical versus basolateral domain specifying
284 activities, then reducing the activity of other apical polarity regulators might partially restore the
285 defects observed in *pac-1; lgl-1* embryos. Two obvious candidates for inactivation are CDC-42 as
286 the presumed target of PAC-1, and aPKC as a major apical domain specifying factor that is
287 counteracted by Lgl.

288 The complete loss of *cdc-42* leads to embryonic lethality. We therefore partially inactivated *cdc-42*
289 using RNAi by bacterial feeding, which causes only ~15% lethality by itself (mostly during
290 embryonic development) (Fig. 4A). To avoid complications from performing double RNAi, we
291 examined the effect of *cdc-42* RNAi on the offspring of *pac-1(mib269); lgl-1(mib201)/lgl-1::GFP*
292 parents. We only counted animals expressing BFP in the pharynx, which are homozygous or
293 heterozygous for the *lgl-1(mib201)* deletion. Consistent with our observation that *lgl-1* loss is
294 partially haplo-insufficient, in control populations 45% of viable offspring expressed BFP (as
295 opposed to the expected 67% if *lgl-1* was not haplo-insufficient) (Fig. 4B). On plates with *cdc-42*
296 RNAi bacteria, the fraction of BFP positive animals increased from 45% to 70% (Fig. 4B).
297 Importantly, when examining adult BFP expressing progeny in detail by confocal microscopy,
298 21/131 did not express any LGL-1::GFP, and were therefore homozygous *pac-1; lgl-1* mutants (Fig.
299 4C, D). Thus, reducing the levels of CDC-42 can partially rescue the embryonic lethality caused by
300 loss of *lgl-1* and *pac-1*.

301 Like CDC-42, the complete loss of aPKC is embryonic lethal. To investigate the effect of reducing
302 aPKC activity on animals lacking LGL-1 and PAC-1, we therefore used the temperature sensitive

303 allele a*PKC(ne4250),* which was contains an H390Q in the kinase domain [57]. We generated an
304 a*PKC(ts); lgl-1(mib201)* double mutant strain and inactivated *pac-1* by dsRNA injection. The
305 reduced aPKC activity at the semi-permissive temperature of 20°C significantly restored
306 embryonic viability of *pac-1(RNAi); lgl-1(mib201)* animals, from 17% in controls to 63% (Fig. 4E). We
307 also investigated the appearance of cell junctions in a*PKC(ts); pac-1(RNAi); lgl-1(mib201)* animals in
308 a strain expressing DLG-1::mCherry as well as an endogenous PAC-1::GFP fusion protein that
309 labels all PAC-1 isoforms (Fig. S4). At the semi-permissive temperature, the reduced aPKC activity
310 rescued the junctional defects of the *pac-1; lgl-1* mutant animals (Fig. 4F). Moreover, the presence
311 of PAC-1::GFP allowed us to rule out that the rescue by *aPKC(ts)* is due to an effect on *pac-1* RNAi
312 efficiency, as we observed the expected strong reduction of PAC-1::GFP signal (Fig. 4F).

313 The rescue of the combined loss of PAC-1 and LGL-1 by reducing the function of CDC-42 or aPKC
314 is consistent with PAC-1 and LGL-1 acting in parallel pathways that both regulate aPKC activity.
315 We therefore wanted to investigate the relative contributions of PAC-1 and LGL-1 to the
316 regulation of aPKC. To accomplish this, we determined whether the loss of PAC-1 or LGL-1
317 individually could compensate for the embryonic lethality associated with partial loss of aPKC or
318 CDC-42. Strikingly, loss of *lgl-1* increased the viability of both *cdc-42(RNAi)* and *aPKC(ts)* embryos,
319 but the loss of *pac-1* had no significant effect (Fig. 4G, H).

320 Taken together our findings support a model in which PAC-1 and LGL-1 act in parallel to antagonize
321 the apical polarizing activities of aPKC and CDC-42. Since individual loss of LGL-1, but not of PAC-
322 1, also suppresses the embryonic lethality of *cdc-42(RNAi)* or *aPKC(ts)* embryos, LGL-1 appears to
323 play a stronger role in the network of inhibitory interactions that establish apical–basal polarity
324 than PAC-1, while PAC-1 may play a more local role at cell junctions.

325

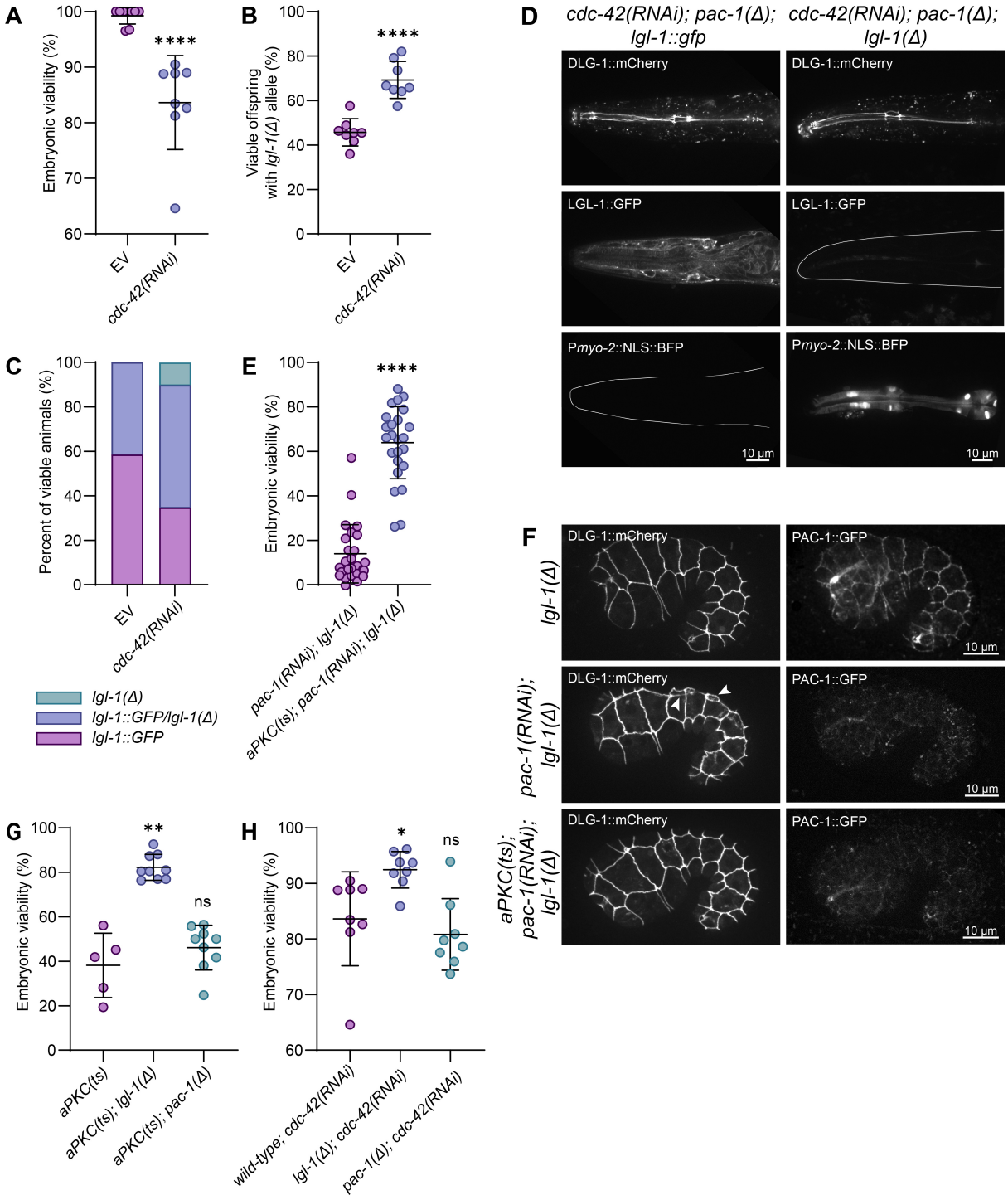

Figure 4. Reduction of CDC-42 or aPKC function rescues the pac-1; lgl-1 embryonic lethality. (**A**) Percentage of viable wild type embryos on empty vector (EV) and cdc-42 RNAi feeding plates. Data is represented as mean ± SD and analyzed with Mann-Whitney test; **** = p <0.0001. (**B**) Percentage of the offspring of *pac-1(mib269); lgl-1(mib201)/lgl-1::gfp* animals on either empty vector or cdc-42 RNAi feeding plates, which contain the *lgl-1(mib201)* allele. Data is represented as mean ± SD and analyzed with unpaired t-test with Welch's correction; **** = p <0.0001. (**C**) Genotype of offspring of *pac-1(mib269); lgl-1(mib201)/lgl-1::gfp* parents on empty vector or cdc-42 RNAi plates. (EV n= 390, *cdc-42*

RNAi n= 254) (**D**) Single plane images of pharyngeal markers showing examples of two genotypes of animals from the cdc-42 RNAi plates. Strain used: BOX1176. (**E**) Percentage of viable *pac-1(RNAi); lgl-1(mib201)* embryos in control and upon the partial reduction of aPKC(ts) activity at the semi-permissive temperature of 20°C. Data is represented as mean ± SD and analyzed with Mann-Whitney test; **** = $p < 0.0001$. (**F**) Maximum intensity projections of 3D stacks taken with a spinning disc confocal microscope showing the localization of DLG-1::mCherry and PAC-1::GFP. Images of PAC-1::GFP were processed using SAIBR for spectral auto fluorescence correction [58]. Arrowheads indicate ectopic basal junctional signals. Strains used: BOX1179, BOX1177. (**G**) Percentage of viable embryos from *aPKC(ts), aPKC(ts); lgl-1(mib201)* or *aPKC(ts); pac-1(mib269)*, at semi-permissive temperature of 20°C. Data is represented as mean ± SD and analyzed with Kruskal-Wallis statistical test with Dunn's multiple comparison test; ns = $p > 0.05$, ** = $p = 0.0012$. (**H**) Percentage of viable embryos from wild-type, *lgl-1(mib201)* or *pac-1(mib269)* on *cdc-42* RNAi. Data is represented as mean ± SD and analyzed with Kruskal-Wallis statistical test with Dunn's multiple comparison test; ns = $p > 0.05$, * = $p = 0.0431$.

Discussion

Here we show that LGL-1 acts redundantly with the RhoGAP protein PAC-1 to control morphogenesis of the embryonic epidermal epithelium of *C. elegans*. Loss of *lgl-1* alone does not cause defects in cell polarization and does not affect viability. Loss of *pac-1* causes defects in cell positioning during gastrulation, but ~90% of embryos recover and hatch with no morphological defects [39,41]. In contrast, the combined loss of *pac-1* and *lgl-1* leads is fully penetrant lethal phenotype. Most animals arrest as embryos around the 2-fold stage of elongation with severe morphological defects in the epidermis, including rupture. These defects are likely caused by a failure to properly polarize epidermal epithelial cells, as we observed an increased apical domain size, defects in the localization of basolateral LET-413^{Scribble}, and severe defects in the positioning of cell junctions.

The severe defects in apical–basal polarization strongly suggest that PAC-1 and LGL-1 act redundantly to control epithelial polarity. At what level do these two proteins act redundantly? A likely candidate is the regulation of aPKC. In flies and mammalian model systems, antagonism between Lgl and aPKC is well established [1–4]. Previous studies in *C. elegans* have implicated LGL-1 as a regulator of aPKC in the zygote and spermatheca. Loss of LGL-1 in one-cell embryos that also lack PAR-2 results in an expansion of the anterior PAR-6–aPKC domain [35,36], and *lgl-1* loss can suppress the sterility observed in a temperature sensitive *aPKC* mutant, which is likely due to junctional defects in the spermatheca [38]. Our genetic analysis now indicates that LGL-1

367 acts as an inhibitor of aPKC activity in the epidermal epithelium. First, the combined loss of PAC-
368 1 and LGL-1 leads to increased apical domain size at the expense of the basolateral domain,
369 phenotypes consistent with overactivation of aPKC. Second, the lethality of combined loss of *pac-*
370 *1* and *lgl-1* can be suppressed by reducing aPKC activity. Finally, loss of *lgl-1* alone suppresses the
371 embryonic lethality of *aPKC(ts)* mutants at the semi-permissive temperature. While additional
372 non-aPKC dependent roles are possible, the predominant function of LGL-1 in the epidermis
373 therefore likely is the inhibition of aPKC. Thus, *C. elegans* LGL-1 has now been shown to act as an
374 inhibitor of aPKC in multiple tissues.

375 PAC-1 was also identified as a regulator of aPKC during radial polarization of *C. elegans*
376 blastomeres. In *pac-1* mutant blastomere stage embryos, PAR-6 and aPKC localize uniformly to
377 the entire cell cortex rather than being enriched at the contact-free apical surface [39].
378 Experiments using constitutively active CDC-42 and PAR-6 mutants unable to bind to CDC-42
379 indicate that PAC-1 locally inactivates CDC-42 at cell–cell contacts to restrict PAR-6–aPKC
380 recruitment to the apical contact-free surface [39]. Inhibition of aPKC activity via downregulation
381 of Cdc42 is further supported by studies of the *Drosophila* PAC-1 ortholog RhoGAP19D. Similar to

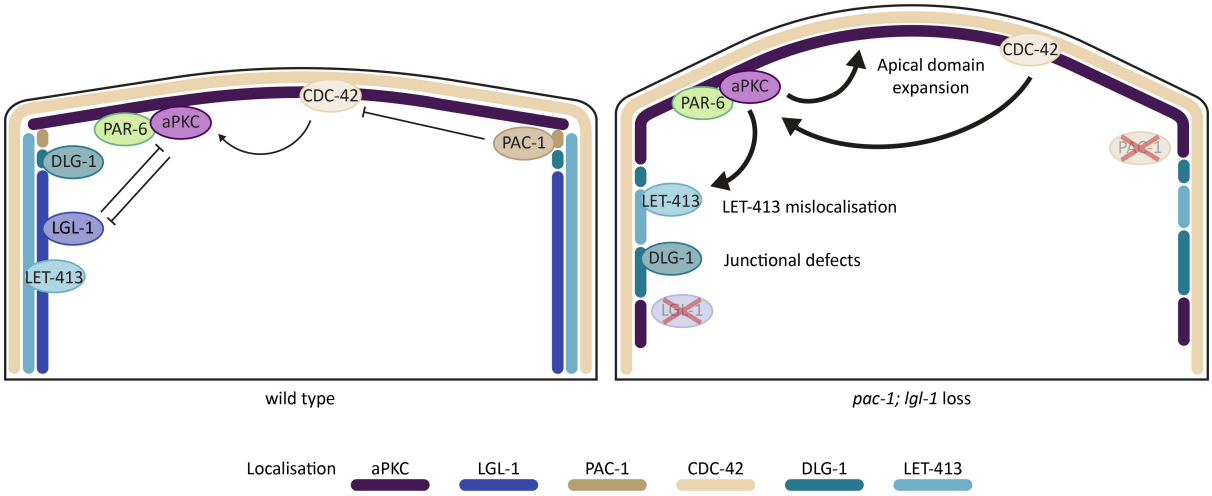

382

383 **Figure 5. Model of LGL-1 and PAC-1 function in the *C. elegans* embryonic epidermal cells.**
384 Colored lines indicate the relative localization of proteins.

385 *C. elegans* blastomeres, RhoGAP19D is recruited to E-cadherin adhesion complexes in the
386 *Drosophila* follicular epithelium, and *rhogap19d* mutants show increased lateral Cdc42 activity
387 together with an expansion of the apical domain due to higher Par6–aPKC activity [42].
388 Moreover, *rhogap19d* mutant follicle cells invade the overlying germline cyst. This phenotype is
389 suppressed by loss of one copy of *aPKC*, and enhanced by loss of one copy of *lgl*, consistent with
390 our genetic analyses [42].

391 Interestingly, the roles of PAC-1 and CDC-42 have previously been investigated in the embryonic
392 epidermis. In that study, PAC-1 and CDC-42 were shown to be involved in regulating junctional
393 actin dynamics and adherens junction protein levels during elongation, but to be dispensable for
394 polarization and junction maturation [41]. Our data examining the roles of PAC-1 and CDC-42 in
395 an *lgl-1* mutant background now demonstrate that both proteins are important regulators of
396 epidermal cell polarity, consistent with the previously described function of PAC-1 in *C. elegans*
397 blastomeres [39], the essential role of CDC-42 regulating aPKC activity in the *C. elegans* zygote
398 [11], and the roles of orthologs of both proteins in other systems. Whether the previously
399 observed defects in actin regulation and adherens junction protein levels reflect aPKC
400 independent functions of CDC-42 and/or PAC-1 or are a manifestation of underlying minor
401 polarity defects remains to be determined. While the defects in polarization and junction
402 establishment are severe, we cannot exclude therefore that non-aPKC dependent roles of CDC-
403 42 and/or PAC-1 contribute to the morphogenesis defects of *pac-1 lgl-1* double mutants.

404 Taken together, the simplest model integrating our findings is that analogous to recent models
405 proposed for *Drosophila*, PAC-1 and LGL-1 act in parallel pathways that oppose aPKC activity (Fig.
406 5). In this model, LGL-1 directly binds to and inhibits PAR-6/aPKC, while PAC-1 indirectly reduces
407 aPKC activity by locally inactivating CDC-42. While the overall mechanisms of epithelial
408 polarization are thus conserved between *C. elegans* and *Drosophila*, important differences still
409 exist. In *C. elegans*, neither LGL-1 nor PAC-1 are essential proteins, whereas Lgl and RhoGAP19D
410 are both individually required for epithelial polarization [24,42,59]. Another difference is the
411 importance of the Crumbs proteins. While the single *Drosophila* Crumbs protein is essential for
412 epithelial polarization [60,61], a triple deletion strain lacking all three *C. elegans crumbs* genes is
413 viable and shows no polarity defects [33]. Nevertheless, minor defects in epithelial organization
414 upon loss of the Crumbs protein CRB-1 can been observed in a mutant background lacking the
415 Scribble ortholog *let-413* and the α-catenin ortholog *hmp-1* [62], and overexpression of the
416 Crumbs protein EAT-20 or CRB-3 in the intestine causes mild enlargement of the apical domain
417 [32]. One interpretation of these differences is that, for reasons remaining to be discovered,
418 regulation of aPKC is more critical in *Drosophila* than in *C. elegans.* Alternatively, the strength of
419 aPKC regulation by RhoGAP19D, Lgl, and Crumbs may be stronger in *Drosophila* than in *C.*
420 *elegans*, such that loss of any regulator more strongly affects overall aPKC activity levels.

421 Redundancy between Lgl and other polarity proteins may not be unique to *C. elegans*. The role of
422 Lgl proteins as negative regulators of aPKC is well established in mammalian models [8,9,63–66].
423 However, whether Lgl is broadly essential for polarity establishment in mammals has been

424 difficult to assess due to the presence of two paralogs, individual knockouts of which cause
425 tissue-specific and late appearing phenotypes. In mice, knockout of Lgl1 specifically affects
426 polarization of neuronal cells, and knockout mice die shortly after birth from severe
427 hydrocephalus [65], while Lgl2 knockout mice are born small due to a placental branching defect
428 but develop into normal adults [67]. In zebrafish, only cell-type specific roles have been reported
429 upon Lgl loss, including neuroepithelial polarity defects for Lgl1 [69] and basal and peridermal
430 formation defects for Lgl2 [66,70,71]. The presence of two paralogs may be an explanation for
431 the lack of more severe defects. However, a recent preprint study generating conditional double
432 knockouts found that mice lacking both *Lgl1* and *Lgl2* in the skin epidermis are viable and fertile
433 [72]. Thus, while the complete absence of polarity phenotypes upon Lgl loss appears unique to *C.*
434 *elegans*, Lgl proteins may well act redundantly with other polarity pathways in vertebrates as
435 well.

436 Finally, while we favor a model based on regulation of aPKC activity by PAC-1 via CDC-42, other
437 interpretations are possible. In the epidermis, degradation of CDC-42 does not block polarization
438 [41]. While apical PAR-6 levels are reduced, PAR-6 is still asymmetrically localized in CDC-42
439 depleted embryos. Thus, additional mechanisms to regulate PAR-6/aPKC localization may remain
440 to be discovered. A recent study of blastomere stage polarization has also suggested that PAC-1
441 may regulate aPKC independently of CDC-42 [73]. Quantitative analysis of aPKC levels showed
442 that the uniform localization of aPKC in *pac-1* mutants is due to a loss of apical aPKC rather than
443 to ectopic lateral recruitment. More importantly, CDC-42 degradation using the ZF1 degron did
444 not prevent aPKC polarization, yet in this CDC-42 depleted background *pac-1* RNAi still caused
445 aPKC to become uniformly localized. These results are inconsistent with PAC-1 acting via CDC-42.
446 As PAC-1 can act as a GAP for other Rho-family small GTPases [74], an alternative hypothesis that
447 was suggested is that PAC-1 acts via a different small GTPase. Our own genetic data cannot
448 elucidate whether PAC-1 acts solely via CDC-42 and aPKC. While the rescue of embryonic lethality
449 of *pac-1 lgl-1* double mutants by partial loss of *cdc-42* or *aPKC* is consistent with this, it was
450 surprising to us that loss of *pac-1* alone did not affect embryonic lethality of *cdc-42(RNAi)* or
451 *aPKC(ts)* animals. This result could be interpreted as PAC-1 not acting in the same pathway as
452 either CDC-42 or aPKC. However, even if PAC-1 were to act in a separate pathway controlling
453 apical–basal polarity, it's loss would still be expected to affect the phenotypes of other mutants
454 in polarity regulators, including CDC-42 or aPKC.

455 One difficulty in resolving the precise relationship between PAC-1, CDC-42, and aPKC is that we
456 cannot directly assess the activity of aPKC, and a currently available CDC-42 biosensor is not very

457 sensitive to small or local changes in CDC-42 activity, due to its strong and uniform cortical
458 localization. Only severe reductions in CDC-42 activity, *e.g.* through *cdc-42(RNAi)* or
459 overexpression of PAC-1, have been reported to result in consistent changes in localization of
460 the biosensor [41,56]. In *Drosophila,* analysis of Cdc42 sensors more clearly support that
461 RhoGAP19D acts via Cdc42, as RhoGAP19D loss results in lateral recruitment of the Cdc42
462 effectors N-WASP and Gek [42]. Moreover, induced recruitment of RhoGAP19D to the apical
463 domain mimics *cdc42* mutants. For these reasons, we consider it likely that PAC-1 does act
464 (predominantly) via CDC-42 and aPKC but plays a smaller role in regulating aPKC activity than
465 LGL-1. As long as LGL-1 is present, the loss of PAC-1 has little effect on aPKC activity.

466 In summary, our study shows that the overall network of proteins regulating epithelial polarity is
467 highly conserved in *C. elegans.* The surprising finding that LGL-1 is a non-essential protein does
468 not reflect an alternative mode of polarization but likely reflects variations in the strengths of
469 connections within this polarity network.

470 Methods

471 *C. elegans* strains and culture conditions

472 *C. elegans* strains were cultured under standard conditions [75]. Only hermaphrodites were used
473 and all experiments, until stated otherwise, were performed with animals grown at 15°C on
474 Nematode Growth Medium (NGM) agar plates seeded with *Escherichia coli* OP50 bacteria. Table 1
475 contains a list of all the strains used. All strains were derived from N2/CGC1.

476 CRISPR

477 The *lgl-1(mib44)* knockout allele and *afd-1(mib34)* knock-in allele, were generated using plasmid-
478 based expression of Cas9 and sgRNA using the self-excising cassette (SEC) for selection [76] and
479 the *lgl-1(mib201)*, *pac-1(mib269)*, *pac-1(mib296)* and *dlg-1(mib128)* were generated using a
480 plasmid-free approach [77]. The *lgl-1(mib44)* edit was made in N2 background and the other edits
481 were made in the CGC1 background. In cases where the sgRNA target site was not disrupted by
482 sequence integration, silent mutations were incorporated to prevent repeated DNA cleavage.
483 The sequences to generate the CRISPR alleles are found in table 2. The full genome sequences of
484 the final strains are available in Supplementary File 1.

485 For the plasmid-based CRISPR/Cas9 editing, the homology arms for *lgl-1(mib44)* were cloned in
486 SapTrap assembly vector pMLS257 [76]. The sgRNAs were expressed from a plasmid under a
487 control of a U6 promoter. To generate sgRNA vectors, antisense oligonucleotide pairs were
488 annealed and ligated into BbsI-linearized pJJR50 (Addgene ID #75026) [78]. Injection mixes were
489 prepared in MilliQ water and contained 50 ng/ml *Peft-3::cas9* (Addgene ID #46168) [79] 50-100
490 ng/ml *U6::sgRNA*, and 50-75 ng/ml of repair template. The mix contained 2.5 ng/ml of the co-
491 injection pharyngeal marker *Pmyo-2::tdTomato* to aid in the visual selection of transgenic strains.
492 Young adult hermaphrodite germlines were microinjected using an inverted microinjection setup
493 (Eppendorft FemtoJet 4x mounted on a Zeiss Axio Observer A. 1 equipped with an Eppendorf
494 Transferman 4r). The candidate edited progeny were selected on plates contain 250 ng/ml of
495 hygromycin [76] and correct genome editing was confirmed by Sanger sequencing (Macrogen).
496 From the correctly edited animals, the hygromycin selection cassette was excised by a heat
497 shock of L1 larvae at 34°C for 1 hour in a water bath.

498 For the knock-in and knockout strains generated using the plasmid-free approach, the repair
499 templates were PCR amplified using Q5 Hot Start Polymerase [77]. The amplification of the
500 repair template was done from the following pre-existing donor vectors: GFP from pJRK86
501 (Addgene ID #173743), BFP from pDD356, and mCherry from pRS004. The generated animals
502 were sequenced for correct gene editing by Sanger sequencing (Macrogen).

503 Genome wide-RNAi screen

504 The RNAi screen was conducted as described in [43]. The administered RNAi feeding used the
505 publicly available Ahringer RNAi clone library [44]. The primary screen was conducted using the
506 NYUAD high-throughput screening automated platform, using the wild-type N2 and *lgl-*
507 *1(mib44)* animals, in two replicates (described in [80]). From the screen, 79 clones caused
508 lethality, developmental delay or arrest, sterility, embryonic lethality or morphological defects in
509 the *lgl-1(mib44)* animals and not or to a lesser extent in the wild-type. 27 of the clones were
510 discarded as false positives, as they are frequently found in other RNAi screens done using the
511 same pipeline. The rest of the 52 clones were independently tested by putting L1 animals on
512 RNAi feeding using sequence verified Ahringer RNAi library clones (see section RNAi treatment).

513 ## RNAi treatment

514 All RNAi clones for the verification screen and targeted experiments were obtained from the
515 genome wide Ahringer HT115 RNAi feeding library, supplied through Source BioScience, and
516 verified using Sanger sequencing.

517 For feeding RNAi experiments, bacteria were pre-cultured in 2–4 ml lysogeny broth (LB)
518 supplemented with 100 µg/ml ampicillin (Amp) and 2.5 µg/ml tetracycline (Tet) at 37°C in an
519 incubator rotating at 220 rpm. Bacteria were then diluted 1:5 in 10 ml LB Amp/Tet for the
520 genome-wide RNAi verification screen or 1:1000 in 25 ml LB Amp/Tet for the *cdc-42* RNAi feeding
521 experiments. To induce production of dsRNA, the cultures were incubated for an hour with 1mM
522 Isoporyl b-D-1-thiogalactopyranoside (IPTG). Bacterial cultures were pelleted by centrifugation at
523 4000 g for 15 minutes at 4°C, and concentrated 5 times. NGM plates were supplemented with
524 100 µg/ml Amp, 2.5 µg/ml Tet and 1 mM IPTG, seeded with 200 µl of bacteria, kept at room
525 temperature for 48 hours in the dark, until dry then kept at 4°C until used.

526 For the *cdc-42* RNAi experiments, young adults were placed on the seeded RNAi plates for 2 days,
527 at 20°C. The following day the number of animals with a visible *lgl-1(mib201)* pharyngeal marker
528 were counted and scored for their genotype based on their fluorescence, using a spinning disc
529 fluorescence microscope.

530 For stronger RNAi, young adults were injected with dsRNA targeting *pac-1* and *lgl-1*. To generate
531 dsRNA, *pac-1* and *lgl-1* clones from the Ahringer RNAi library were amplified using Q5 Hot Start
532 High-Fidelity DNA polymerase (New England Biolabs). The PCR product was used as a template
533 for in vitro dsRNA synthesis using MEGAscript T7 transcription kit (ThermoFisher Scientific).
534 dsRNA was diluted 1:5 in RNase free water prior to micro-injection, and kept at -80°C. The
535 injected animals were kept at 15°C for 24 hours, then transferred to new plates and used for
536 lethality assays.

537 ## Embryonic viability and lethality assays

538 Young adult animals were cultured at 15°C on OP50 plates, and allowed to lay eggs for 24–36
539 hours. Animals were subsequently removed and after 24 hours the number of hatched or
540 unhatched eggs was counted. Embryos that did not hatch and young dead larvae were counted
541 as dead. For *aPKC(ts)* experiments young adults were allowed to lay eggs at the permissive
542 temperature of 15°C for 20 hours, then were moved to a semi-permissive temperature of 20°C

543 for 8 hours. The adults were then taken off and the embryos were left to hatch at 20°C for 24
544 hours before counting viability.

545 Imaging

546 Imaging of *C. elegans* was done by mounting embryos or larvae on a 5% agarose pad in a 10 mM
547 Tetramizole solution in M9 buffer to induce paralysis. DIC imaging was performed using an
548 upright Zeiss Axio Imager Z2 microscope using a 100x 1.4 NA objective and Zeiss AxioCam 503
549 monochrome camera, driven by Zeiss Zen Blue Software. Spinning disc confocal imaging was
550 performed using a Nikon Ti-U microscope driven by MetaMorph Microscopy Automation and
551 Image Analysis Software (Molecular Devices) and equipped with Yokogawa CSU-X1-M1 confocal
552 head and a Prime BSI sCMOS camera (Teledyne Photometrics), using Nikon CFI Plan Apo λ 60 x
553 or 100 x 1.4 NA objectives. AiryScan imaging was done using Confocal Laser Scanning
554 microscope Zeiss LSM980 AiryScan 2 Axio Observer 7 SP with Definite Focus 3, driven by ZEN
555 Blue v3.9, using Alpha Plan-APO 100 x objective and Axiocam 305 mono R2 camera.

556 Time-lapse imaging for FRAP experiments was performed using a Nikon Eclipse Ti-E microscope
557 driven by MetaMorph Microscopy Automation and Image Analysis Software (Molecular Devices)
558 and equipped with Yokagawa CSU-X1-A1 confocal Spinning Disc unit and Prime BSI sCMOS
559 camera (Teledyne Photometrics), using a Plan Apo VC 100x 1.4 NA objective. Targeted
560 photobleaching was done using an ILas system (Roper Scientific France/PICT-IBiSA, Institute
561 Curie).

562 All stacks were obtained at 0.25 µm intervals. Images were analyzed and processed using Fiji and
563 Imaris. For quantifications, the same laser power, exposure times and z-stack sizes were used
564 within experiments. Time-lapse stacks of developing embryos were acquired every 5 minutes for
565 4.75 hours. Images of PAC-1::GFP were processed using SAIBR for spectral auto fluorescence
566 correction using the default settings [58]. Images of GFP::ABD_{VAB-10} were processed using
567 unsharp mask, radius (Sigma) 1.0 pixels, mask weight 0.60.

568 Fluorescence recovery after photobleaching (FRAP)

569 For FRAP assays, laser power was adjusted in each experiment to avoid complete
570 photobleaching of the selected area. Photobleaching of epidermal DLG-1 was performed using a
571 consistent laser setting for all animals and a photobleached area of ~50 pixels in width. Time-
572 lapse images were taken prior, during, and immediately after photobleaching. Recovery was

573 followed at 1 s intervals for 200 s. Time-lapse movies were analyzed in Fiji. A 20 pixel wide line
574 was drawn over the middle of the bleached area defined by the bleached region in the first post-
575 bleach frame. For each time-lapse frame, the maximum intensity value within the bleached
576 region was determined, and the background, defined by the mean intensity of a non-bleached
577 region outside of the animal, was subtracted. The maximum intensities within the bleached
578 region were corrected for acquisition photobleaching per frame using the background-
579 subtracted maximum intensity of a similar non-bleached junction. FRAP recovery was calculated
580 as the change in the corrected intensity values within the bleached region. The first frame after
581 bleach was defined as 0% and the average maximum intensity of 8 frames before bleaching as
582 100%.

583 Apical curvature measurement

584 Apical curvature measurements were done using PH::GFP as a membrane marker. To measure
585 the apical curvature of the epidermal cells, a free hand line was drawn over the apical domain of
586 as many cells in a row as possible, defined as cells with clearly distinguishable apical and lateral
587 domains (minimum 10 cells). Then a segmented line was drawn from junction to junction for the
588 same cells. The length of the apical domain line was divided by the length of the junction-to-
589 junction line, giving one curvature value per embryo.

590 CDC-42 biosensor apical intensity measurements

591 To measure the CDC-42 biosensor intensity at the apical domain of the seam cells, a maximum
592 intensity projection of a 3D stack covering the apical domain of the cells was generated. For cells
593 with a clearly visible outline, a polygon selection tool was used to outline the area of the apical
594 domain, as big as possible for every cell, that did not include the signal from the junctions. For
595 each cell, the mean value was determined and background intensity from an area outside the
596 embryo subtracted. The values were averaged for the whole embryo.

597 Statistical analysis

598 All statistical analysis was done using GraphPad Prism 10. For populations comparisons, a
599 D'Agostino & Pearson test of normality was first performed to determine if the data was sampled
600 from a Gaussian distribution. For data drawn from a Gaussian distribution, comparisons
601 between two populations were done using an unpaired t test (with Welch's correction if the
602 standard deviations of the populations differed significantly), and for data that was not normally

603 distributed, a Mann-Whitney test was performed. For multiple comparisons tests, for data drawn
604 from Gaussian distribution, but with significantly different standard deviations, the Brown-
605 Forsythe and Welch ANOVA test followed by Dunnett's T3 multiple comparison test was used and
606 for non-normally distributed data the Kruskal-Wallis test followed by Dunn's multiple pairwise
607 comparison test was performed.

608 Tables

609 **Table 1. List of *C. elegans* strains used in the study.**

Reagent type (species) or resource	**Designation**	**Genotype**	**Source or reference**
Strain, strain background (*C. elegans*)	PD1074	wild-type	CGC
Strain, strain background (*C. elegans*)	FT1459	*xnIs506 [Pcdc42::GST::GFP::wsp-1(GBD) + unc-119(+)]*	[41]
Strain, strain background (*C. elegans*)	PE97	*hmp-1(fe4[S823F]) V*	[53]
Strain, strain background (*C. elegans*)	WM151	*pkc-3(ne4250 [E9K; H390Q]) II*	Gift from Rodriguez lab
Strain, strain background (*C. elegans*)	BOX258	*afd-1(mib34[afd-1::GFP-LoxP]) I*	This study
Strain, strain background (*C. elegans*)	BOX527	*mibIs49[Pwrt-2::TIR-1::tagBFP2-LoxP::tbb-2-3'UTR, IV:5014740-5014802 (cxTi10816 site)]) IV; mib29[let-413::mCherry-LoxP]) V; dlg-1(mib35[dlg-1::AID::GFP-LoxP]) X*	[81]
Strain, strain background (*C. elegans*)	BOX804	*hmr-1(he298[hmr-1::GFP]) I; mibIs49[Pwrt-2::TIR-1::tagBFP2-LoxP::tbb-2-3'UTR, IV:5014740..5014802 (cxTi10816 site)]) IV; dlg-1(mib128[dlg-1::AID::mCherry-LoxP]) X*	This study
Strain, strain background (*C. elegans*)	BOX899	*lgl-1(mib201[Pmyo-2::NLS::mTagBFP2, X:863693..874171]) dlg-1(mib23[dlg-1::mCherry-LoxP]) X*	This study
Strain, strain background (*C. elegans*)	BOX907	*pac-1(mib269[III: 8494328..8519244]) III*	This study
Strain, strain background (*C. elegans*)	BOX919	*lgl-1(mib201[Pmyo-2::NLS::mTagBFP2, X:863693..874171]) X*	This study

Strain, strain background (*C. elegans*)	BOX921	*cxTi10816(he259[Peft-3::PH::GFP::LOV::tbb-2]; lgl-1(mib201[Pmyo-2::NLS::mTagBFP2, X:863693..874171]) X*	This study, PH::GFP from [82]
Strain, strain background (*C. elegans*)	BOX940	*hmr-1(he298[hmr-1::GFP]) I; lgl-1(mib201[Pmyo-2::NLS::mTagBFP2, X:863693..874171]) dlg-1(mib128[dlg-1::AID::mCherry-LoxP]) X*	This study
Strain, strain background (*C. elegans*)	BOX943	*afd-1(mib34[afd-1::GFP-LoxP]) I; lgl-1(mib201[Pmyo-2::NLS::mTagBFP2, X:863693..874171]) X*	This study
Strain, strain background (*C. elegans*)	BOX975	*mcIs50 [Plin-26::vab-10(actin-binding domain)::GFP + Pmyo-2::GFP + pBluescript]; lgl-1(mib201[Pmyo-2::NLS::mTagBFP2, X:863693..874171]) X*	This study
Strain, strain background (*C. elegans*)	BOX976	*mcIs50 [Plin-26::vab-10(actin-binding domain)::GFP + Pmyo-2::GFP + pBluescript]*	This study, backcrossed from ML1735
Strain, strain background (*C. elegans*)	BOX990	*ajm-1(ouIs20[ajm-1::mCherry + unc-119+]); lgl-1(mib201[Pmyo-2::NLS::mTagBFP2, X:863693..874171]) dlg-1(mib22[dlg-1::GFP-LoxP]) X*	This study
Strain, strain background (*C. elegans*)	BOX992	*xnIs506 [Pcdc42::GST::GFP::wsp-1(GBD) + unc-119(+)]; lgl-1(mib201[Pmyo-2::NLS::mTagBFP2, X:863693..874171]) X*	This study
Strain, strain background (*C. elegans*)	BOX1027	*pkc-3(ne4250 [E9K; H390Q]) II; lgl-1(mib201[Pmyo-2::NLS::mTagBFP2, X:863693..874171]) X*	This study
Strain, strain background (*C. elegans*)	BOX1076	*cxTi10816(he259[Peft-3::PH::GFP::LOV::tbb-2]); dlg-1(mib23[dlg-1::mCherry-LoxP]) X*	This study
Strain, strain background (*C. elegans*)	BOX1077	*cxTi10816(he259[Peft-3::PH::GFP::LOV::tbb-2]); lgl-1(mib201[Pmyo-2::NLS::mTagBFP2, X:863693..874171]) dlg-1(mib23[dlg-1::mCherry-LoxP]) X*	This study
Strain, strain background (*C. elegans*)	BOX1100	*let-413 (mib29[let-413::mCherry-LoxP]) V/+; dlg-1(mib35[dlg-1::AID::GFP-LoxP]) lgl-1(mib201[Pmyo-2::NLS::mTagBFP2, X:863693..874171]) X*	This study
Strain, strain background (*C. elegans*)	BOX1111	*pac-1(mib269[III: 8494328..8519244]) III; lgl-1(crk66[lgl-1::GFP]) /lgl-1(mib201[Pmyo-2::NLS::mTagBFP2, X:863693..874171]) X*	This study, lgl-1::GFP from [58]
Strain, strain background (*C. elegans*)	BOX1161	*pkc-3(mib78[GFP-LoxP::AID::pkc-3]) II; lgl-1(mib201[Pmyo-2::NLS::mTagBFP2, X:863693..874171]) dlg-1(mib23[dlg-1::mCherry-LoxP]) X*	This study, pkc-3 from [54]
Strain, strain background (*C. elegans*)	BOX1162	*pkc-3(mib78[GFP-LoxP::AID::pkc-3]) II; dlg-1(mib23[dlg-1::mCherry-LoxP]) X*	This study, dlg-1 from [83]

Strain, strain background (*C. elegans*)	BOX1176	*pac-1(mib269[III: 8494328..8519244]) III; lgl-1(crk66[lgl-1::GFP])/lgl-1(mib201[Pmyo-2::NLS::mTagBFP2, X:863693..874171]) dlg-1(mib23[dlg-1::mCherry-LoxP])/+ X*	This study
Strain, strain background (*C. elegans*)	BOX1177	*pkc-3(ne4250 [E9K; H390Q]) II; pac-1(mib296[pac-1::mIAA7::GFP])III; lgl-1(mib201[Pmyo-2::NLS::mTagBFP2, X:863693..874171]) X; dlg-1(mib23[dlg-1::mCherry-LoxP]) X*	This study
Strain, strain background (*C. elegans*)	BOX1179	*pac-1(mib296[pac-1::mIAA7::GFP]) III; lgl-1(mib201[Pmyo-2::NLS::mTagBFP2, X:863693..874171]) dlg-1(mib23[dlg-1::mCherry-LoxP]) X*	This study
Strain, strain background (*C. elegans*)	BOX1195	*pkc-3(ne4250 [E9K; H390Q]) II; pac-1(mib269[III: 8494328..8519244]) III*	This study
Strain, strain background (*C. elegans*)	BOX1221	*pac-1(mib269[III: 8494328..8519244]) III; lgl-1(mib201[Pmyo-2::NLS::mTagBFP2, X:863693..874171]) X/+*	This study

610 **Table 2. List of guide RNA and primers used to generate the CRISPR edited animals.**

Reagents to generate *lgl-1(mib44)*		**Sequence source**
crRNA		
N-terminal		
sgRNA forward primer	TCTTGTATAAGATCACTGCGCTGGA	Wormbase
sgRNA reverse primer	AAACTCCAGCGCAGTGATCTTATA	Wormbase
C-terminal		
sgRNA forward primer	AAACGAGGAGCATGCCATAGAACA	Wormbase
sgRNA reverse primer	TCTTGTGTTCTATGGCATGCTCCTC	Wormbase
Repair template primers		
Left arm		
Forward primer	GGCTGCTCTTCGTGGCAGTGCAGTAGCAGCAGCA	Wormbase
Reverse primer	GGGTGCTCTTCGCATCTCGGGTTCGTGATAAAACTTG	Wormbase
Right arm		
Forward primer	GGCTGCTCTTCGGGTGAAGGGCTGAAGATCAAAAA	Wormbase
Reverse primer	GGGTGCTCTTCGTACGCCACCTATGCGTTGACCTTT	Wormbase
Reagents to generate *lgl-1(mib201)*		**Sequence source**
crRNA		
N-terminal	TCTCCTTTACTCATggtcga	Wormbase
C-terminal	TGCTGGGATTACACATGGCA	Wormbase
Repair template primers		
Forward	cttctctccaccacttttcatttttaccctcgaccATGCCAGCCGCCAAGCGTGTCAAGCTCGACATGGTTTCGGAATTGATTAA	Wormbase
Reverse	GAGAGAAACGAGATGGAATTAGAGCAGTTGATCTAGTTGAGCTTGTGTCCGAGCT	Wormbase

Repair template	ATGCCAGCCGCCAAGCGTGTCAAGCTCGACATGGTTT CGGAATTGATTAAGGAAAATATGCACATGAAGCTCTA CATGGAGGGAACCGTCGACAACCACCACTTCAAGTGC ACCTCCGAGGGAGAGGGAAAGCCATACGAGGGAACCC AAACCATGCGTATCAAGGTCGTCGAGGGAGGACCACT CCCATTCGCCTTCGACATCCTCGCCACCTCCTTCCTC TACGGATCCAAGgtaagtttaaacatatatatactaa ctaaccctgattatttaaattttcagACCTTCATCAA CCACACCCAAGGAATCCCAGACTTCTTCAAGCAATCC TTCCCAGAGGGATTCACCTGGGAGCGTGTCACCACCT ACGAGGACGGAGGAGTCCTCACCGCCACCCAAGACAC CTCCCTCCAAGACGGATGCCTCATCTACAACGTCAAG gtaagtttaaacagttcggtactaactaaccatacat atttaaattttcagATCCGTGGAGTCAACTTCACCTC CAACGGACCAGTCATGCAAAAGAAGACCCTCGGATGG GAGGCCTTCACCGAGACCCTCTACCCAGCCGACGGAG GACTCGAGGGACGTAACGACATGGCCCTCAAGCTCGT CGGAGGATCCCACCTCATCGCCAACGCCAAGgtaagt ttaaacatgattttactaactaactaatctgatttaa attttcagACCACCTACCGTTCCAAGAAGCCAGCCAA GAACCTCAAGATGCCAGGAGTCTACTACGTCGACTAC CGTCTCGAGCGTATCAAGGAGGCCAACAACGAGACCT ACGTCGAGCAACACGAGGTCGCCGTCGCCCGTTACTG CGACCTCCCATCCAAGCTCGGACACAAGCTCAACTAG	Wormbase
Reagents to generate *pac-1(mib269)*		**Sequence source**
crRNA		
N-terminal	acgcactttttgatgctcaa	Wormbase
C-terminal	atcctttcgtacctccggta	Wormbase
Repair template	tatcggtacacctcaactacgcacttttgatgctgt atgggtttcttctcctcatttctccattcattt	Wormbase
Reagents to generate *pac-1(mib296)*		**Sequence source**
crRNA		
C-terminal	AAGCGATGTTGATACTTTGA	Wormbase
Repair template primers		
Forward	CTGCCAGACGACACACGTTAAGCGATGTTGATACTGG ATTCTCCGAGACCGTCG	Wormbase
Reverse	ctttaacacttttatttcaatatttctgggattacCT TCAACTTGTAGAGCTCGTCCATTCCG	Wormbase
Reagents to generate *dlg-1(mib128)*		**Sequence source**
crRNA		
N-terminal	CTCAGGAGCATCGATGTCCA	Wormbase
C-terminal	CGGAATGGACGAGCTCTACA	Wormbase
Repair template primers		
Forward	aggcggcggcgttcgtgaagTCCTCAGGAGCATCGAT GTCCAAGGGAGAGGAGGAC	Wormbase
Reverse	aaacttacCTTTCCGGATTGAAAGTACAGATTCTCCT TGTAGAGCTCGTCCATTCCTC	Wormbase
Reagents to generate *afd-1(mib34)*		**Sequence source**
crRNA		
C-terminal		
sgRNA forward primer	TTGGAATTATGGCTTTTGCGGGG	Wormbase
sgRNA reverse primer	AACCCCCGCAAAAGCCATAATTC	Wormbase
Repair template primers		

Left arm		
Forward primer	GGCTGCTCTTCGTGGCATCTCGATGCACCAAGATTGAC	Wormbase
Reverse primer	GGGTGCTCTTCGCGCTGGCTTTTGCGGGGTGGCGG	Wormbase
Right arm		
Forward primer	CTGCTCTTCGACGTAATTCTTATGTATTTTTAAAGAAAATTGTTTTTTCAC	Wormbase
Reverse primer	GTGCTCTTCGTACGATCTCCGAACCCTAAGAAATTGTCC	Wormbase

Author contributions

Olga D. Jarosińska: Conceptualization, Formal analysis, Investigation, Writing - Original Draft, Writing - Review & Editing, Visualization. **Amalia Riga:** Conceptualization, Formal analysis, Investigation, Writing - Review & Editing. **Hala Zahreddine Fahs:** Investigation, Supervision, Writing - Review & Editing. **Joren M. Woeltjes:** Investigation, Writing - Review & Editing. **Ruben Schmidt:** Investigation, Writing - Review & Editing. **Fathima S. Refai:** Investigation, Writing - Review & Editing. **Suma Gopinadhan:** Investigation, Writing - Review & Editing. **Kristin C. Gunsalus:** Supervision, Writing - Review & Editing, Funding acquisition. **Mike Boxem:** Conceptualization, Writing - Original Draft, Writing - Review & Editing, Supervision, Funding acquisition.

Acknowledgements

We thank members of the M. Boxem, S. van den Heuvel, S. Ruijtenberg, S. Suijkerbuijk and L. Braccioli groups for helpful discussions. We thank J. Nance, M. Labouesse, J. Rodriguez, N. Goehring, for strains and reagents. We thank the NYUAD Core Technology Platforms, in particular Nikolas Giakoumidis and Reza Rowshan, for assistance with the NYUAD high-throughput screening facility, and Nabil Rahiman for the RNAi screen scoring database. We also thank Wormbase [84] and the Biology Imaging Center, Faculty of Sciences, Department of Biology, Utrecht University. Some strains were provided by the Caenorhabditis Genetics Center, which is funded by NIH Office of Research Infrastructure Programs (P40 OD010440). This work was supported by the European Union's Horizon 2020 research and innovation programme under the Marie Skłodowska-Curie grant agreement No. 675407 – PolarNet; Dutch Research

634 Council (NWO) grant 016.VICI.170.165; and by Tamkeen under the NYU Abu Dhabi Research
635 Institute Award to the NYUAD Center for Genomics and Systems Biology (ADHPG-CGSB).

Bibliography

1. **Buckley C.E. and St Johnston D.** Apical–basal polarity and the control of epithelial form and function. *Nat Rev Mol Cell Biol.* **23**: 559–577 (2022). https://doi.org/10.1038/s41580-022-00465-y

2. **Campanale J.P., Sun T.Y., and Montell D.J.** Development and dynamics of cell polarity at a glance. *J Cell Sci.* **130**: 1201–1207 (2017). https://doi.org/10.1242/jcs.188599

3. **Rodriguez-Boulan E. and Macara I.G.** Organization and execution of the epithelial polarity programme. *Nat Rev Mol Cell Biol.* **15**: 225–242 (2014). https://doi.org/10.1038/nrm3775

4. **St Johnston D. and Ahringer J.** Cell polarity in eggs and epithelia: parallels and diversity. *Cell.* **141**: 757–774 (2010). https://doi.org/10.1016/j.cell.2010.05.011

5. **Betschinger J., Mechtler K., and Knoblich J.A.** The Par complex directs asymmetric cell division by phosphorylating the cytoskeletal protein Lgl. *Nature.* **422**: 326–330 (2003). https://doi.org/10.1038/nature01486

6. **Hong Y.** aPKC: the Kinase that Phosphorylates Cell Polarity. *F1000Research.* **7**: F1000 Faculty Rev-903 (2018). https://doi.org/10.12688/f1000research.14427.1

7. **Hurov J.B., Watkins J.L., and Piwnica-Worms H.** Atypical PKC phosphorylates PAR-1 kinases to regulate localization and activity. *Curr Biol CB.* **14**: 736–741 (2004). https://doi.org/10.1016/j.cub.2004.04.007

8. **Yamanaka T., Horikoshi Y., Sugiyama Y., Ishiyama C., Suzuki A., Hirose T., Iwamatsu A., Shinohara A., and Ohno S.** Mammalian Lgl Forms a Protein Complex with PAR-6 and aPKC Independently of PAR-3 to Regulate Epithelial Cell Polarity. *Curr Biol.* **13**: 734–743 (2003). https://doi.org/10.1016/S0960-9822(03)00244-6

9. **Yamanaka T., Horikoshi Y., Izumi N., Suzuki A., Mizuno K., and Ohno S.** Lgl mediates apical domain disassembly by suppressing the PAR-3-aPKC-PAR-6 complex to orient apical membrane polarity. *J Cell Sci.* **119**: 2107–2118 (2006). https://doi.org/10.1242/jcs.02938

10. **Graybill C., Wee B., Atwood S.X., and Prehoda K.E.** Partitioning-defective Protein 6 (Par-6) Activates Atypical Protein Kinase C (aPKC) by Pseudosubstrate Displacement*. *J Biol Chem.* **287**: 21003–21011 (2012). https://doi.org/10.1074/jbc.M112.360495

664 11. **Rodriguez J., Peglion F., Martin J., Hubatsch L., Reich J., Hirani N., Gubieda A.G., Roffey**
665 **J., Fernandes A.R., St Johnston D., Ahringer J., and Goehring N.W.** aPKC Cycles between
666 Functionally Distinct PAR Protein Assemblies to Drive Cell Polarity. *Dev Cell.* **42**: 400-415.e9
667 (2017). https://doi.org/10.1016/j.devcel.2017.07.007

668 12. **Yamanaka T., Horikoshi Y., Suzuki A., Sugiyama Y., Kitamura K., Maniwa R., Nagai Y.,**
669 **Yamashita A., Hirose T., Ishikawa H., and Ohno S.** PAR-6 regulates aPKC activity in a
670 novel way and mediates cell-cell contact-induced formation of the epithelial junctional
671 complex. *Genes Cells.* **6**: 721–731 (2001). https://doi.org/10.1046/j.1365-2443.2001.00453.x

672 13. **Achilleos A., Wehman A.M., and Nance J.** PAR-3 mediates the initial clustering and apical
673 localization of junction and polarity proteins during C. elegans intestinal epithelial cell
674 polarization. *Dev Camb Engl.* **137**: 1833–1842 (2010). https://doi.org/10.1242/dev.047647

675 14. **Atwood S.X., Chabu C., Penkert R.R., Doe C.Q., and Prehoda K.E.** Cdc42 acts downstream
676 of Bazooka to regulate neuroblast polarity through Par-6/aPKC. *J Cell Sci.* **120**: 3200–3206
677 (2007). https://doi.org/10.1242/jcs.014902

678 15. **Dong W., Lu J., Zhang X., Wu Y., Lettieri K., Hammond G.R., and Hong Y.** A polybasic
679 domain in aPKC mediates Par6-dependent control of membrane targeting and kinase
680 activity. *J Cell Biol.* **219**: e201903031 (2020). https://doi.org/10.1083/jcb.201903031

681 16. **Holly R.W., Jones K., and Prehoda K.E.** A Conserved PDZ-Binding Motif in aPKC Interacts
682 with Par-3 and Mediates Cortical Polarity. *Curr Biol CB.* **30**: 893-898.e5 (2020).
683 https://doi.org/10.1016/j.cub.2019.12.055

684 17. **Lin D., Edwards A.S., Fawcett J.P., Mbamalu G., Scott J.D., and Pawson T.** A mammalian
685 PAR-3–PAR-6 complex implicated in Cdc42/Rac1 and aPKC signalling and cell polarity. *Nat*
686 *Cell Biol.* **2**: 540–547 (2000). https://doi.org/10.1038/35019582

687 18. **McCaffrey L.M. and Macara I.G.** The Par3/aPKC interaction is essential for end bud
688 remodeling and progenitor differentiation during mammary gland morphogenesis. *Genes*
689 *Dev.* **23**: 1450–1460 (2009). https://doi.org/10.1101/gad.1795909

690 19. **Martin-Belmonte F., Gassama A., Datta A., Yu W., Rescher U., Gerke V., and Mostov K.**
691 PTEN-Mediated Apical Segregation of Phosphoinositides Controls Epithelial Morphogenesis
692 through Cdc42. *Cell.* **128**: 383–397 (2007). https://doi.org/10.1016/j.cell.2006.11.051

693 20. **Nunes de Almeida F., Walther R.F., Pressé M.T., Vlassaks E., and Pichaud F.** Cdc42
694 defines apical identity and regulates epithelial morphogenesis by promoting apical
695 recruitment of Par6-aPKC and Crumbs. *Development.* **146**: dev175497 (2019).
696 https://doi.org/10.1242/dev.175497

697 21. **Peterson F.C., Penkert R.R., Volkman B.F., and Prehoda K.E.** Cdc42 Regulates the Par-6
698 PDZ Domain through an Allosteric CRIB-PDZ Transition. *Mol Cell.* **13**: 665–676 (2004).
699 https://doi.org/10.1016/S1097-2765(04)00086-3

700 22. **Qiu R.-G., Abo A., and Martin G.S.** A human homolog of the *C. elegans* polarity
701 determinant Par-6 links Rac and Cdc42 to PKCζ signaling and cell transformation. *Curr Biol.*
702 **10**: 697–707 (2000). https://doi.org/10.1016/S0960-9822(00)00535-2

703 23. **Whitney D.S., Peterson F.C., Kittell A.W., Egner J.M., Prehoda K.E., and Volkman B.F.**
704 Binding of Crumbs to the Par-6 CRIB-PDZ Module Is Regulated by Cdc42. *Biochemistry.* **55**:
705 1455–1461 (2016). https://doi.org/10.1021/acs.biochem.5b01342

706 24. **Bilder D., Li M., and Perrimon N.** Cooperative Regulation of Cell Polarity and Growth by
707 *Drosophila* Tumor Suppressors. *Science.* **289**: 113–116 (2000).
708 https://doi.org/10.1126/science.289.5476.113

709 25. **Hutterer A., Betschinger J., Petronczki M., and Knoblich J.A.** Sequential Roles of Cdc42,
710 Par-6, aPKC, and Lgl in the Establishment of Epithelial Polarity during *Drosophila*
711 Embryogenesis. *Dev Cell.* **6**: 845–854 (2004). https://doi.org/10.1016/j.devcel.2004.05.003

712 26. **Tanentzapf G. and Tepass U.** Interactions between the crumbs, lethal giant larvae and
713 bazooka pathways in epithelial polarization. *Nat Cell Biol.* **5**: 46–52 (2003).
714 https://doi.org/10.1038/ncb896

715 27. **Almagor L. and Weis W.I.** Polarity protein Par6 facilitates the processive phosphorylation
716 of Lgl via a dynamic interaction with aPKC. *Commun Biol.* **8**: 967 (2025).
717 https://doi.org/10.1038/s42003-025-08401-4

718 28. **Earl C.P., Cobbaut M., Barros-Carvalho A., Ivanova M.E., Briggs D.C., Morais-de-Sá E.,**
719 **Parker P.J., and McDonald N.Q.** Capture, mutual inhibition and release mechanism for
720 aPKC–Par6 and its multisite polarity substrate Lgl. *Nat Struct Mol Biol.* **32**: 729–739 (2025).
721 https://doi.org/10.1038/s41594-024-01425-0

722 29. **Herranz H., Stamataki E., Feiguin F., and Milán M.** Self-refinement of Notch activity
723 through the transmembrane protein Crumbs: modulation of γ-Secretase activity. *EMBO Rep.*
724 **7**: 297–302 (2006). https://doi.org/10.1038/sj.embor.7400617

725 30. **Richardson E.C.N. and Pichaud F.** Crumbs is required to achieve proper organ size control
726 during Drosophila head development. *Development.* **137**: 641–650 (2010).
727 https://doi.org/10.1242/dev.041913

728 31. **Tepaß U. and Knust E.** Phenotypic and developmental analysis of mutations at thecrumbs
729 locus, a gene required for the development of epithelia inDrosophila melanogaster. *Rouxs*
730 *Arch Dev Biol.* **199**: 189–206 (1990). https://doi.org/10.1007/bf01682078

731 32. **Castiglioni V.G., Ramalho J.J., Kroll J., Stucchi R., Van Beuzekom H., Schmidt R.,**
732 **Altelaar M., and Boxem M.** Characterization of the composition and functioning of the
733 Crumbs complex in *C. elegans*. Developmental Biology; 2021.
734 https://doi.org/10.1101/2021.08.10.455623

735 33. **Waaijers S., Ramalho J.J., Koorman T., Kruse E., and Boxem M.** The C. elegans Crumbs
736 family contains a CRB3 homolog and is not essential for viability. *Biol Open.* **4**: 276–284
737 (2015). https://doi.org/10.1242/bio.201410744

738 34. **Chen J., Sayadian A.-C., Lowe N., Lovegrove H.E., and St Johnston D.** An alternative
739 mode of epithelial polarity in the Drosophila midgut. *PLoS Biol.* **16**: e3000041 (2018).
740 https://doi.org/10.1371/journal.pbio.3000041

741 35. **Beatty A., Morton D., and Kemphues K.** The C. elegans homolog of Drosophila Lethal
742 giant larvae functions redundantly with PAR-2 to maintain polarity in the early embryo.
743 *Development.* **137**: 3995–4004 (2010). https://doi.org/10.1242/dev.056028

744 36. **Hoege C., Constantinescu A.-T., Schwager A., Goehring N.W., Kumar P., and Hyman**
745 **A.A.** LGL Can Partition the Cortex of One-Cell *Caenorhabditis elegans* Embryos into Two
746 Domains. *Curr Biol.* **20**: 1296–1303 (2010). https://doi.org/10.1016/j.cub.2010.05.061

747 37. **Boyd L., Guo S., Levitan D., Stinchcomb D.T., and Kemphues K.J.** PAR-2 is asymmetrically
748 distributed and promotes association of P granules and PAR-1 with the cortex in C. elegans
749 embryos. *Development.* **122**: 3075–3084 (1996). https://doi.org/10.1242/dev.122.10.3075

750 38. **Montoyo-Rosario J.G., Armenti S.T., Zilberman Y., and Nance J.** The Role of pkc-3 and
751 Genetic Suppressors in Caenorhabditis elegans Epithelial Cell Junction Formation. *Genetics.*
752 **214**: 941–959 (2020). https://doi.org/10.1534/genetics.120.303085

753 39. **Anderson D.C., Gill J.S., Cinalli R.M., and Nance J.** Polarization of the C. elegans Embryo
754 by RhoGAP-Mediated Exclusion of PAR-6 from Cell Contacts. *Science.* **320**: 1771–1774 (2008).
755 https://doi.org/10.1126/science.1156063

756 40. **Klompstra D., Anderson D.C., Yeh J.Y., Zilberman Y., and Nance J.** An instructive role for
757 C. elegans E-cadherin in translating cell contact cues into cortical polarity. *Nat Cell Biol.* **17**:
758 726–735 (2015). https://doi.org/10.1038/ncb3168

759 41. **Zilberman Y., Abrams J., Anderson D.C., and Nance J.** Cdc42 regulates junctional actin
760 but not cell polarization in the *Caenorhabditis elegans* epidermis. *J Cell Biol.* **216**: 3729–3744
761 (2017). https://doi.org/10.1083/jcb.201611061

762 42. **Fic W., Bastock R., Raimondi F., Los E., Inoue Y., Gallop J.L., Russell R.B., and St**
763 **Johnston D.** RhoGAP19D inhibits Cdc42 laterally to control epithelial cell shape and prevent
764 invasion. *J Cell Biol.* **220**: e202009116 (2021). https://doi.org/10.1083/jcb.202009116

765 43. **Cipriani P.G. and Piano F.** RNAi Methods and Screening: RNAi Based High-Throughput
766 Genetic Interaction Screening. *Methods in Cell Biology.* Elsevier; pp. 89–1112011.
767 https://doi.org/10.1016/B978-0-12-544172-8.00004-9

768 44. **Kamath R.S., Fraser A.G., Dong Y., Poulin G., Durbin R., Gotta M., Kanapin A., Le Bot N.,**
769 **Moreno S., Sohrmann M., Welchman D.P., Zipperlen P., and Ahringer J.** Systematic
770 functional analysis of the Caenorhabditis elegans genome using RNAi. *Nature.* **421**: 231–237
771 (2003). https://doi.org/10.1038/nature01278

772 45. **Chan E. and Nance J.** Mechanisms of CDC-42 activation during contact-induced cell
773 polarization. *J Cell Sci.* **126**: 1692–1702 (2013). https://doi.org/10.1242/jcs.124594

774 46. **Bossinger O., Klebes A., Segbert C., Theres C., and Knust E.** Zonula Adherens Formation
775 in *Caenorhabditis elegans* Requires *dlg-1*, the Homologue of the *Drosophila* Gene *discs large*.
776 *Dev Biol.* **230**: 29–42 (2001). https://doi.org/10.1006/dbio.2000.0113

777 47. **Köppen M., Simske J.S., Sims P.A., Firestein B.L., Hall D.H., Radice A.D., Rongo C., and**
778 **Hardin J.D.** Cooperative regulation of AJM-1 controls junctional integrity in Caenorhabditis
779 elegans epithelia. *Nat Cell Biol.* **3**: 983–991 (2001). https://doi.org/10.1038/ncb1101-983

780 48. **Shao X., Lucas B., Strauch J., and Hardin J.** The adhesion modulation domain of
781 *Caenorhabditis elegans* α-catenin regulates actin binding during morphogenesis. Fehon R,
782 editor. *Mol Biol Cell.* **30**: 2115–2123 (2019). https://doi.org/10.1091/mbc.E19-01-0018

783 49. **Cox-Paulson E.A., Walck-Shannon E., Lynch A.M., Yamashiro S., Zaidel-Bar R., Eno C.C.,**
784 **Ono S., and Hardin J.** Tropomodulin protects α-catenin-dependent junctional-actin
785 networks under stress during epithelial morphogenesis. *Curr Biol CB.* **22**: 1500–1505 (2012).
786 https://doi.org/10.1016/j.cub.2012.06.025

787 50. **Pasti G. and Labouesse M.** Epithelial junctions, cytoskeleton, and polarity. *WormBook.* : 1–
788 35 (2014). https://doi.org/10.1895/wormbook.1.56.2

789 51. **Lynch A.M., Grana T., Cox-Paulson E., Couthier A., Cameron M., Chin-Sang I., Pettitt J.,**
790 **and Hardin J.** A Genome-wide Functional Screen Shows MAGI-1 Is an L1CAM-Dependent
791 Stabilizer of Apical Junctions in C. elegans. *Curr Biol.* **22**: 1891–1899 (2012).
792 https://doi.org/10.1016/j.cub.2012.08.024

793 52. **Maiden S.L., Harrison N., Keegan J., Cain B., Lynch A.M., Pettitt J., and Hardin J.** Specific
794 Conserved C-terminal Amino Acids of Caenorhabditis elegans HMP-1/α-Catenin Modulate F-
795 actin Binding Independently of Vinculin*. *J Biol Chem.* **288**: 5694–5706 (2013).
796 https://doi.org/10.1074/jbc.M112.438093

797 53. **Pettitt J., Cox E.A., Broadbent I.D., Flett A., and Hardin J.** The *Caenorhabditis elegans* p120
798 catenin homologue, JAC-1, modulates cadherin–catenin function during epidermal
799 morphogenesis. *J Cell Biol.* **162**: 15–22 (2003). https://doi.org/10.1083/jcb.200212136

800 54. **Castiglioni V.G., Pires H.R., Rosas Bertolini R., Riga A., Kerver J., and Boxem M.**
801 Epidermal PAR-6 and PKC-3 are essential for larval development of C. elegans and organize
802 non-centrosomal microtubules. Hobert O, Pfeffer SR, editors. *eLife.* **9**: e62067 (2020).
803 https://doi.org/10.7554/eLife.62067

804 55. **Kagami M., Toh-e A., and Matsui Y.** Sro7p, a Saccharomyces cerevisiae Counterpart of the
805 Tumor Suppressor l(2)gl Protein, Is Related to Myosins in Function. *Genetics.* **149**: 1717–
806 1727 (1998). https://doi.org/10.1093/genetics/149.4.1717

807 56. **Kumfer K.T., Cook S.J., Squirrell J.M., Eliceiri K.W., Peel N., O'Connell K.F., and White**
808 **J.G.** CGEF-1 and CHIN-1 Regulate CDC-42 Activity during Asymmetric Division in the
809 Caenorhabditis elegans Embryo. *Mol Biol Cell.* **21**: 266–277 (2010).
810 https://doi.org/10.1091/mbc.E09-01-0060

811 57. **Fievet B.T., Rodriguez J., Naganathan S., Lee C., Zeiser E., Ishidate T., Shirayama M.,**
812 **Grill S., and Ahringer J.** Systematic genetic interaction screens uncover cell polarity
813 regulators and functional redundancy. *Nat Cell Biol.* **15**: 103–112 (2013).
814 https://doi.org/10.1038/ncb2639

815 58. **Rodrigues N.T.L., Bland T., Borrego-Pinto J., Ng K., Hirani N., Gu Y., Foo S., and**
816 **Goehring N.W.** SAIBR: a simple, platform-independent method for spectral
817 autofluorescence correction. *Dev Camb Engl.* **149**: dev200545 (2022).
818 https://doi.org/10.1242/dev.200545

819 59. **Jacob L., Opper M., Metzroth B., Phannavong B., and Mechler B.M.** Structure of the *l(2)gl*
820 gene of Drosophila and delimitation of its tumor suppressor domain. *Cell.* **50**: 215–225
821 (1987). https://doi.org/10.1016/0092-8674(87)90217-0

822 60. **Bulgakova N.A. and Knust E.** The Crumbs complex: from epithelial-cell polarity to retinal
823 degeneration. *J Cell Sci.* **122**: 2587–2596 (2009). https://doi.org/10.1242/jcs.023648

824 61. **Médina E., Lemmers C., Lane-Guermonprez L., and Le Bivic A.** Role of the Crumbs
825 complex in the regulation of junction formation in Drosophila and mammalian epithelial
826 cells. *Biol Cell.* **94**: 305–313 (2002). https://doi.org/10.1016/S0248-4900(02)00004-7

827 62. **Segbert C., Johnson K., Theres C., van Fürden D., and Bossinger O.** Molecular and
828 functional analysis of apical junction formation in the gut epithelium of *Caenorhabditis*
829 *elegans*. *Dev Biol.* **266**: 17–26 (2004). https://doi.org/10.1016/j.ydbio.2003.10.019

830 63. **Chalmers A.D., Pambos M., Mason J., Lang S., Wylie C., and Papalopulu N.** aPKC,
831 Crumbs3 and Lgl2 control apicobasal polarity in early vertebrate development.
832 *Development.* **132**: 977–986 (2005). https://doi.org/10.1242/dev.01645

833 64. **Dodd M.E., Hatzold J., Mathias J.R., Walters K.B., Bennin D.A., Rhodes J., Kanki J.P.,**
834 **Look A.T., Hammerschmidt M., and Huttenlocher A.** The ENTH domain protein Clint1 is
835 required for epidermal homeostasis in zebrafish. *Development.* **136**: 2591–2600 (2009).
836 https://doi.org/10.1242/dev.038448

837 65. **Klezovitch O., Fernandez T.E., Tapscott S.J., and Vasioukhin V.** Loss of cell polarity
838 causes severe brain dysplasia in Lgl1 knockout mice. *Genes Dev.* **18**: 559–571 (2004).
839 https://doi.org/10.1101/gad.1178004

840 66. **Sonawane M., Martin-Maischein H., Schwarz H., and Nüsslein-Volhard C.** Lgl2 and E-
841 cadherin act antagonistically to regulate hemidesmosome formation during epidermal
842 development in zebrafish. *Development.* **136**: 1231–1240 (2009).
843 https://doi.org/10.1242/dev.032508

844 67. **Sripathy S., Lee M., and Vasioukhin V.** Mammalian *Llgl2* Is Necessary for Proper
845 Branching Morphogenesis during Placental Development. *Mol Cell Biol.* **31**: 2920–2933
846 (2011). https://doi.org/10.1128/MCB.05431-11

847 68. Mammalian Llgl2 Is Necessary for Proper Branching Morphogenesis during Placental
848 Development. [cited 22 Jun 2025]. Available:
849 https://www.tandfonline.com/doi/epdf/10.1128/MCB.05431-11?needAccess=true

850 69. **Clark B.S., Cui S., Miesfeld J.B., Klezovitch O., Vasioukhin V., and Link B.A.** Loss of Llgl1
851 in retinal neuroepithelia reveals links between apical domain size, Notch activity and
852 neurogenesis. *Dev Camb Engl.* **139**: 1599–1610 (2012). https://doi.org/10.1242/dev.078097

853 70. **Raman R., Damle I., Rote R., Banerjee S., Dingare C., and Sonawane M.** aPKC regulates
854 apical localization of Lgl to restrict elongation of microridges in developing zebrafish
855 epidermis. *Nat Commun.* **7**: 11643 (2016). https://doi.org/10.1038/ncomms11643

856 71. **Sonawane M., Carpio Y., Geisler R., Schwarz H., Maischein H.-M., and Nuesslein-**
857 **Volhard C.** Zebrafish penner/lethal giant larvae 2 functions in hemidesmosome formation,
858 maintenance of cellular morphology and growth regulation in the developing basal
859 epidermis. *Dev Camb Engl.* **132**: 3255–3265 (2005). https://doi.org/10.1242/dev.01904

860 72. **Bii V.M., Rudoy D., Klezovitch O., and Vasioukhin V.** Lethal giant larvae gene family (Llgl1
861 and Llgl2) functions as a tumor suppressor in mouse skin epidermis. *BioRxiv Prepr Serv Biol.*
862 : 2023.03.06.531408 (2023). https://doi.org/10.1101/2023.03.06.531408

863 73. **Stolpner N.J., Manzi N.I., Su T., and Dickinson D.J.** Apical PAR protein caps orient the
864 mitotic spindle in C. elegans early embryos. *Curr Biol CB.* **33**: 4312-4329.e6 (2023).
865 https://doi.org/10.1016/j.cub.2023.08.069

866 74. **Chen W., Blanc J., and Lim L.** Characterization of a promiscuous GTPase-activating protein
867 that has a Bcr-related domain from Caenorhabditis elegans. *J Biol Chem.* **269**: 820–823
868 (1994). https://doi.org/10.1016/S0021-9258(17)42184-3

869 75. **Brenner S.** The genetics of Caenorhabditis elegans. *Genetics.* **77**: 71–94 (1974).
870 https://doi.org/10.1093/genetics/77.1.71

871 76. **Dickinson D.J., Pani A.M., Heppert J.K., Higgins C.D., and Goldstein B.** Streamlined
872 Genome Engineering with a Self-Excising Drug Selection Cassette. *Genetics.* **200**: 1035–1049
873 (2015). https://doi.org/10.1534/genetics.115.178335

874 77. **Ghanta K.S. and Mello C.C.** Melting dsDNA Donor Molecules Greatly Improves Precision
875 Genome Editing in Caenorhabditis elegans. *Genetics.* **216**: 643–650 (2020).
876 https://doi.org/10.1534/genetics.120.303564

877 78. **Waaijers S., Muñoz J., Berends C., Ramalho J.J., Goerdayal S.S., Low T.Y., Zoumaro-**
878 **Djayoon A.D., Hoffmann M., Koorman T., Tas R.P., Harterink M., Seelk S., Kerver J.,**
879 **Hoogenraad C.C., Bossinger O., Tursun B., van den Heuvel S., Heck A.J.R., and Boxem**
880 **M.** A tissue-specific protein purification approach in Caenorhabditis elegans identifies novel
881 interaction partners of DLG-1/Discs large. *BMC Biol.* **14**: 66 (2016).
882 https://doi.org/10.1186/s12915-016-0286-x

883 79. **Friedland A.E., Tzur Y.B., Esvelt K.M., Colaiácovo M.P., Church G.M., and Calarco J.A.**
884 Heritable genome editing in C. elegans via a CRISPR-Cas9 system. *Nat Methods.* **10**: 741–743
885 (2013). https://doi.org/10.1038/nmeth.2532

886 80. **Fahs H.Z., Refai F.S., Gopinadhan S., Moussa Y., Gan H.H., Hunashal Y., Battaglia G.,**
887 **Cipriani P.G., Ciancia C., Rahiman N., Kremb S., Xie X., Pearson Y.E., Butterfoss G.L.,**
888 **Maizels R.M., Esposito G., Page A.P., Gunsalus K.C., and Piano F.** A new class of natural

anthelmintics targeting lipid metabolism. *Nat Commun.* **16**: 305 (2025). https://doi.org/10.1038/s41467-024-54965-w

81. **Riga A., Cravo J., Schmidt R., Pires H.R., Castiglioni V.G., Van Den Heuvel S., and Boxem M.** Caenorhabditis elegans LET-413 Scribble is essential in the epidermis for growth, viability, and directional outgrowth of epithelial seam cells. Nance J, editor. *PLOS Genet.* **17**: e1009856 (2021). https://doi.org/10.1371/journal.pgen.1009856

82. **Fielmich L.-E., Schmidt R., Dickinson D.J., Goldstein B., Akhmanova A., and Van Den Heuvel S.** Optogenetic dissection of mitotic spindle positioning in vivo. *eLife.* 2018. https://doi.org/10.7554/eLife.38198

83. **Kroll J.R., Remmelzwaal S., and Boxem M.** CeLINC, a fluorescence-based protein-protein interaction assay in Caenorhabditis elegans. *Genetics.* **219**: iyab163 (2021). https://doi.org/10.1093/genetics/iyab163

84. **Sternberg P.W., Van Auken K., Wang Q., Wright A., Yook K., Zarowiecki M., Arnaboldi V., Becerra A., Brown S., Cain S., Chan J., Chen W.J., Cho J., Davis P., Diamantakis S., Dyer S., Grigoriadis D., Grove C.A., Harris T., et al.** WormBase 2024: status and transitioning to Alliance infrastructure. *Genetics.* **227**: iyae050 (2024). https://doi.org/10.1093/genetics/iyae050